

Global Biogeochemical Cycles



REVIEW ARTICLE

10.1029/2020GB006775

Key Points:

- Review of oceanic distribution, controlling processes, and sedimentary archives of carbon (C), nitrogen (N), and silicon (Si) isotopes
- Late Quaternary C, N, and Si sedimentary isotope records demonstrate coupling between ocean carbon and nutrient cycling and atmospheric CO₂ levels
- Cenozoic C, N, and Si sedimentary isotope records indicate large-scale changes in nutrient sources, concentrations, and the carbon cycle

Assessment of C, N, and Si Isotopes as Tracers of Past Ocean Nutrient and Carbon Cycling

J. R. Farmer^{1,2} , J. E. Hertzberg³ , D. Cardinal⁴ , S. Fietz⁵ , K. Hendry⁶ , S. L. Jaccard^{7,8} , A. Paytan⁹ , P. A. Rafter¹⁰ , H. Ren¹¹ , C. J. Somes¹² , J. N. Sutton¹³ , and GEOTRACES PAGES Biological Productivity Working Group Members¹⁴

¹Department of Geosciences, Princeton University, Princeton, NJ, USA, ²Max-Planck Institute for Chemistry, Mainz, Germany, ³International Ocean Discovery Program, Texas A&M University, College Station, TX, USA, ⁴LOCEAN (UMR7159), Sorbonne Université, IRD, CNRS, MNHN, Paris, France, ⁵Department of Earth Sciences, Stellenbosch University, Stellenbosch, South Africa, ⁶School of Earth Sciences, University of Bristol, Bristol, UK, ⁷Institute of Geological Sciences and Oeschger Center for Climate Change Research, University of Bern, Bern, Switzerland, ⁸Institute of Earth Sciences, University of Lausanne, Lausanne, Switzerland, ⁹Institute of Marine Sciences, University of California, Santa Cruz, Santa Cruz, CA, USA, ¹⁰Department of Earth System Science, University of California, Irvine, CA, USA, ¹¹Department of Geosciences, National Taiwan University, Taipei, Taiwan, ¹²GEOMAR Helmholtz Centre for Ocean Research Kiel, Kiel, Germany, ¹³University of Brest, CNRS, IRD, Ifremer, Institut Universitaire Européen de la Mer, LEMAR, Plouzané, France, ¹⁴A full list of working group members and their affiliations appears at the Appendix A

Correspondence to:

J. R. Farmer and J. E. Hertzberg,
jesse.farmer@princeton.edu;
hertzberg@iodp.tamu.edu

Citation:

Farmer, J. R., Hertzberg, J. E., Cardinal, D., Fietz, S., Hendry, K., Jaccard, S. L., et al. (2021). Assessment of C, N, and Si isotopes as tracers of past ocean nutrient and carbon cycling. *Global Biogeochemical Cycles*, 35, e2020GB006775. <https://doi.org/10.1029/2020GB006775>

Received 13 AUG 2020
 Accepted 14 MAY 2021

Abstract Biological productivity in the ocean directly influences the partitioning of carbon between the atmosphere and ocean interior. Through this carbon cycle feedback, changing ocean productivity has long been hypothesized as a key pathway for modulating past atmospheric carbon dioxide levels and hence global climate. Because phytoplankton preferentially assimilate the light isotopes of carbon and the major nutrients nitrate and silicic acid, stable isotopes of carbon (C), nitrogen (N), and silicon (Si) in seawater and marine sediments can inform on ocean carbon and nutrient cycling, and by extension the relationship with biological productivity and global climate. Here, we compile water column C, N, and Si stable isotopes from GEOTRACES-era data in four key ocean regions to review geochemical proxies of oceanic carbon and nutrient cycling based on the C, N, and Si isotopic composition of marine sediments. External sources and sinks as well as internal cycling (including assimilation, particulate matter export, and regeneration) are discussed as likely drivers of observed C, N, and Si isotope distributions in the ocean. The potential for C, N, and Si isotope measurements in sedimentary archives to record aspects of past ocean C and nutrient cycling is evaluated, along with key uncertainties and limitations associated with each proxy. Constraints on ocean C and nutrient cycling during late Quaternary glacial-interglacial cycles and over the Cenozoic are examined. This review highlights opportunities for future research using multielement stable isotope proxy applications and emphasizes the importance of such applications to reconstructing past changes in the oceans and climate system.

Plain Language Summary The ability of marine phytoplankton to fix carbon—and hence influence the air-sea partitioning of the greenhouse gas carbon dioxide—highlights the potential for these organisms to influence global climate in the past and future. In addition to C, phytoplankton require nutrients including inorganic N and for certain groups, Si. Because nutrients fuel phytoplankton growth, tracing past nutrient uptake can inform on important aspects of past biological production. Phytoplankton preferentially incorporate the light isotopes of C, N, and Si into their cells and metabolic products. These isotopic signatures can be preserved in marine sediments, providing a means to reconstruct past changes in biological activity. Here we use new data to illuminate processes driving the stable isotopic composition of C, N, and Si in the water column and in marine sediments. We evaluate the processes that lead to changes in the concentration of these elements and their isotopes in the ocean. We discuss scientific caveats and the extent of uncertainty relevant for interpreting past records of these isotopes. We then discuss examples of representative geochemical reconstructions using sediment records from the last ice age and over the last 70 million years. We use this knowledge to highlight directions for future research.

© 2021. The Authors.

This is an open access article under the terms of the [Creative Commons Attribution-NonCommercial License](https://creativecommons.org/licenses/by-nc/4.0/), which permits use, distribution and reproduction in any medium, provided the original work is properly cited and is not used for commercial purposes.

1. Introduction

Within the sunlit surface ocean, photoautotrophs (“phytoplankton”) use sunlight to assimilate C via photosynthesis, acquire nutrients, and convert these inorganic constituents to biogenic material (organic matter and biogenic minerals). This biogenic material, which forms the base of the oceanic food web, is either regenerated (“recycled” via microbial respiration or mineral dissolution) to release dissolved inorganic elements within the shallow surface ocean or sinks and is exported to depths below the mixed layer. In the deep ocean, exported biogenic material is largely (but not wholly) regenerated, and the resulting regenerated inorganic elements eventually return to the surface ocean via upwelling and mixing. The remaining biogenic material that is not regenerated in the water column will be removed via burial into surface sediments, where regeneration will continue and only a small fraction will be preserved. This interplay of inorganic element supply, biological assimilation, recycling, export, and burial defines what we call the “wheel” of ocean productivity (Box 1; see Sigman & Hain, 2012).

The ocean productivity “wheel” has long been recognized to impact the stable isotopic composition of many bioactive elements in seawater and in marine sediments (e.g., Abelson & Hoering, 1961; De La Rocha et al., 1997; Fogel & Cifuentes, 1993; Tappan, 1968; Wada, 1980). Conceptually, phytoplankton preferentially assimilate the light isotope of many dissolved bioactive elements. This preference leads to higher concentrations of the heavy isotope in the residual dissolved element pools, which consequently become isotopically heavy (Figure 1). At the same time, the newly formed biogenic material is depleted in the heavy isotope of these bioactive elements, that is, the biogenic material is isotopically lighter. Regeneration of biogenic material in the deep ocean contributes to an isotopically light deep ocean pool of dissolved bioactive elements (Figure 1). The fraction of this exported biogenic material that is buried in the sediments retains its light isotopic signature. At steady state, the loss of biogenic material into the sediments must be counterbalanced by external supply of new bioactive elements to the ocean (Figure 1).

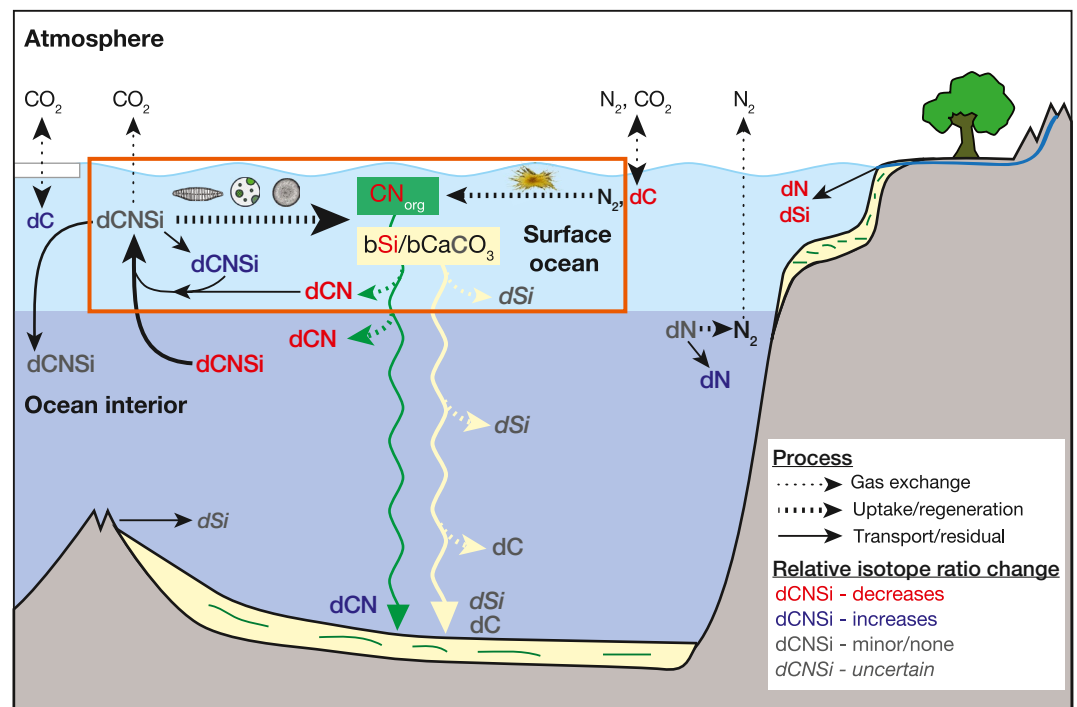


Figure 1. Schematic summary of processes affecting the isotopic composition of dissolved C, N, and Si (dCNSi). Processes related to biological productivity are outlined in the orange box. Gas exchange processes are indicated by dotted arrows; uptake and regeneration follow dashed arrows. Solid arrows indicate dissolved element transport due to ocean circulation or sinking, or the residual dissolved element pool resulting from incomplete consumption during uptake. Red/blue/gray/italicized elements denote a relative decrease/increase/minor/uncertain change to the isotopic composition (δ -value) of the element resulting from the associated process. Basemap modified after Hain et al. (2014).

Box 1. Surface Ocean Productivity, Deep Ocean Nutrients, and Paleoproductivity

Several terms define the magnitude of different components of ocean productivity (Bender et al., 1987; Sigman & Hain, 2012). Net primary production (NPP) refers to the rate of production by photoautotrophs minus their metabolic requirements (or their respiration); it is effectively the rate at which phytoplankton produce new biomass (green curve in euphotic zone of Figure 2). Net ecosystem production (NEP) is NPP minus the total (ecosystem) respiration. When functionally constrained to the euphotic zone, at steady state, NEP equates to *export production*; that is, NEP equates to the removal of organic material from the euphotic zone (undulating green line in Figure 2). Hereafter, we will use NEP and export production interchangeably. Integrated over the entire ocean and on sufficiently long timescales, at steady state NEP (i.e., removal) must equal the biological uptake of new nutrients in the surface ocean (delivered via upwelling, mixing, and external sources).

NEP is of profound interest to paleoclimate research, as NEP provides a mechanism to remove C from the surface ocean and thus away from direct contact with the atmosphere. C export from the surface ocean prevents C regeneration in the euphotic zone, which in turn lowers the concentration of CO₂ in the surface ocean. This increases CO₂ solubility and thus lowers the partial pressure of atmospheric carbon dioxide (*p*CO₂). This process, termed the *biological pump* (Volk & Hoffert, 1985), acts to reduce *p*CO₂ over time intervals ranging from the mixing timescale of the intermediate and deep ocean (decades to millennia) at minimum, to geologic timescales for exported carbon preserved in the sediments (millennia to millions of years).

Regarding the biological pump's ability to impact *p*CO₂, two parameters are of primary importance: (a) the *efficiency of the biological pump* and (b) *nutrient utilization rates*. An understanding of these parameters requires assessing the origins of nutrients in the deep ocean. In the deep ocean, nutrients are present as either *regenerated* from (largely microbial) decomposition of biogenic material (brown arrow in Figure 2) or *preformed* from the sinking and transport of surface waters with unused nutrient concentrations via deep ocean thermohaline circulation (yellow arrow in Figure 2). The *strength of the biological pump* is simply the average concentration of regenerated nutrients in the deep ocean (Hain et al., 2014). A stronger biological pump is one with higher C transport to the deep ocean (i.e., NEP is higher). The regeneration of this transported organic C at depth leads to a greater abundance of C and regenerated nutrients in the deep ocean.

However, a stronger biological pump in isolation does not necessarily lower *p*CO₂. Instead, the operative term for *p*CO₂ is the *efficiency of the biological pump*. This efficiency is defined by the ratio of regenerated to preformed nutrients in the deep ocean. In ocean biogeochemical models, a greater fraction of regenerated nutrients in the deep ocean indicates a more efficient biological pump and is associated with lower *p*CO₂ (Ito & Follows, 2005; Marinov et al., 2006; Matsumoto, 2007). The efficiency of the biological pump is intimately related to the nutrient status of surface waters in deep water formation regions because these regions set the balance of preformed and regenerated nutrients in the deep ocean (Figure 2). The term *nutrient utilization* defines this nutrient status as the fractional biological assimilation of available nutrients relative to their supply to the euphotic zone (annually integrated).

Note that nutrient utilization is not necessarily coupled to NEP. Consider three cases motivated by studies of the Southern Ocean over glacial-interglacial cycles (Section 7.1): an initial case with low nutrient utilization and low NEP, and two alterations of this initial case where nutrient utilization increases (Figure 2). In the first altered case, higher nutrient utilization occurs because of greater biological assimilation of the same nutrient supply (Figure 2b). This could happen because of alleviation of a micronutrient limitation (for instance, from greater iron input). In this scenario, NEP would increase, and the biological pump would be more efficient. However, consider a second altered case where nutrient utilization increases because of a reduction in nutrient supply (Figure 2c), for instance, due to reduced vertical exchange (e.g., a more stratified ocean). In this second

case, NEP could either stay the same or even decrease, but the biological pump would still be more efficient. For these reasons, knowledge of past changes in NEP and nutrient utilization in the high latitude oceans are critical to testing hypotheses of changes in $p\text{CO}_2$ (Berger et al., 1989; Broecker, 1982; Galbraith & Jaccard, 2015; Galbraith & Skinner, 2020; Hain et al., 2014; Paytan, 2009; Sigman et al., 2010).

Much as biological productivity serves as an overarching concept including multiple key variables, *paleoproductivity* is a similarly broad concept encompassing reconstructions of multiple parameters relevant to biological productivity. These include, but are not limited to, proxies for the accumulation of organic debris within sediments (Paytan, 2009), flux normalization tools (Costa et al., 2020), and sedimentary redox conditions (Tribovillard et al., 2006). Here, our focus lies on nutrient isotope tracers. As described in Section 3, these tools are sensitive to past nutrient utilization and thus inform on past partitioning between preformed and regenerated nutrient pools.

This conceptual framework has motivated numerous studies on the stable isotopes of carbon and major nutrients—particularly nitrogen (N) isotopes of nitrate and silicon (Si) isotopes of silicic acid—as tracers related to ocean biological processes. Phosphate is also a critical major nutrient, but aside from oxygen isotopes in phosphate (e.g., Paytan & McLaughlin, 2011), phosphorous has only one stable isotope and is not discussed here. There are numerous pathways, both internal and external, that influence the isotopic composition of C, N, and Si in the ocean (Figure 1). Furthermore, the distributions of C, N, and Si isotopes in their dominant dissolved inorganic forms are incompletely sampled in today's ocean and are only accessible in past oceans through proxies in marine sediments. Thus, deciphering information on past biological activity in the ocean requires understanding both the processes controlling the distribution and isotopic composition of dissolved inorganic C, N, and Si, and how signatures of these processes are preserved in marine sediments.

Here we review the primary controls on C, N, and Si stable isotopes in the water column and in marine sediments. Although these isotope systems have been utilized by the paleoceanographic community for decades, a timely review is warranted given the expanded number of water column isotope profiles (especially for N and Si) alongside new developments in the analysis and interpretation of marine sediment archives. Our work relies on new data collected by the GEOTRACES program, an international survey of the marine

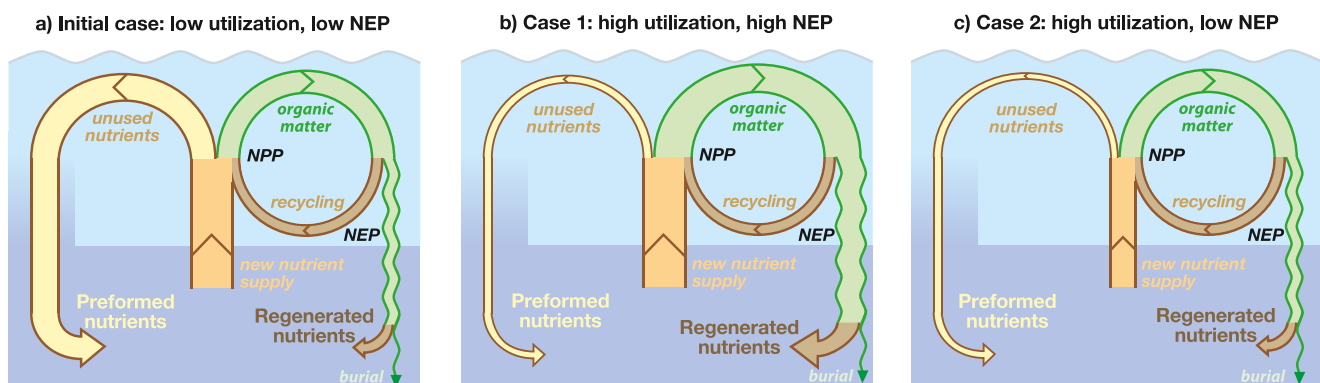


Figure 2. Three hypothetical cases linking surface ocean productivity with deep ocean nutrients. Light blue color indicates the euphotic zone; dark blue indicates the deep ocean. In the initial case (a), most of the new nutrient supply is subducted without being used. NEP is low, deep ocean preformed nutrients are high, regenerated nutrients are low, and the biological pump is inefficient. In case 1 (b), most of the new nutrient supply goes to NEP. NEP is high, deep ocean preformed nutrients are low, regenerated nutrients are high, and the biological pump is more efficient. In case 2 (c), the new nutrient supply is lower, and the same quantity of NEP occurs as in the initial case. Here NEP is low, but deep ocean preformed nutrients are also low, regenerated nutrients are high, and the biological pump is more efficient. For simplicity, the recycling and burial fluxes are assumed constant in all scenarios. Figure inspired by Sigman & Hain (2012). NEP, net ecosystem production; NPP, net primary production.

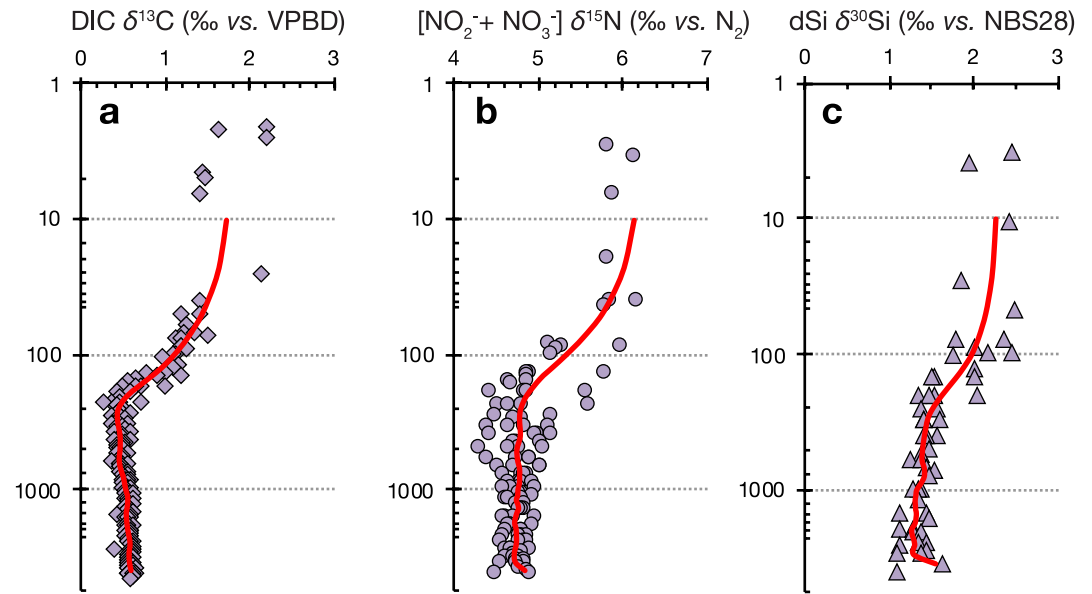


Figure 3. Interpolated spline fits to Antarctic Zone water column data for $\delta^{13}\text{C}_{\text{DIC}}$ (a, diamonds), $[\text{NO}_2^- + \text{NO}_3^-] \delta^{15}\text{N}$ (b, circles), and $\text{dSi} \delta^{30}\text{Si}$ (c, triangles). Data sources: (a) CLIVAR P16S (Feely et al., 2008), (b) CLIVAR P16S (Rafter et al., 2013), (c) GEOTRACES GIPY04 stations 57, 62, 72, and 78 (Fripiat et al., 2012).

biogeochemical cycling of elements and their isotopes (Anderson, 2020), and particularly the GEOTRACES 2017 Intermediate Data Product (IDP2017, Schlitzer et al., 2018) that includes isotope data of many dissolved constituents in seawater from 39 cruises collected between 2007 and 2014. We focus specifically on C, N, and Si, while a synthesis of bioactive trace elements and their isotopes is provided in a companion manuscript (Horner et al., 2021).

The manuscript is outlined as follows. Section 2 provides background on isotope notation and data sources used throughout. Section 3 defines common processes affecting C, N, and Si isotopes. Sections 4–6 review the modern water column distribution, driving processes, sediment archives, and sources of uncertainty for paleo reconstructions from C, N, and Si isotopes, respectively. Section 7 presents two case studies where C, N, and Si isotopes provide foundational constraints for understanding past C and nutrient cycling on short (glacial-interglacial) and long (Cenozoic) timescales.

2. Data Notations and Sources

2.1. Reporting of Isotope Ratios

Isotope ratios are reported in δ notation, expressing the deviation in sample isotope ratio relative to accepted international standards of known isotopic composition (Coplen, 2011):

$$\delta^{13}\text{C} = \frac{\left(\frac{^{13}\text{C}}{^{12}\text{C}} \right)_{\text{sample}} - \left(\frac{^{13}\text{C}}{^{12}\text{C}} \right)_{\text{VPDB}}}{\left(\frac{^{13}\text{C}}{^{12}\text{C}} \right)_{\text{VPDB}}} \quad (1)$$

$$\delta^{15}\text{N} = \frac{\left(\frac{^{15}\text{N}}{^{14}\text{N}} \right)_{\text{sample}} - \left(\frac{^{15}\text{N}}{^{14}\text{N}} \right)_{\text{air N}_2}}{\left(\frac{^{15}\text{N}}{^{14}\text{N}} \right)_{\text{air N}_2}} \quad (2)$$

$$\delta^{30}\text{Si} = \frac{\left(\frac{^{30}\text{Si}}{^{28}\text{Si}} \right)_{\text{sample}} - \left(\frac{^{30}\text{Si}}{^{28}\text{Si}} \right)_{\text{NBS28}}}{\left(\frac{^{30}\text{Si}}{^{28}\text{Si}} \right)_{\text{NBS28}}} \quad (3)$$

where VPBD (Coplen et al., 2006), air N₂ (Mariotti, 1983), and NBS28 (Coplen et al., 2002) are the accepted international standards for C, N, and Si isotopes, respectively. By convention, δ values are multiplied by 10³ and reported in parts-per-thousand (‰).

2.2. Data Sources

Seawater data presented here are sourced from four oceanographic regions of distinct hydrography, biogeochemistry, and export production: The North Atlantic Subtropical Gyre (hereafter NASTG), the eastern tropical South Pacific (hereafter ETSP), the central tropical South Pacific (hereafter CTSP), and the Southern Ocean. Southern Ocean data are further subdivided into the Subantarctic Zone (hereafter SAZ), between the Subtropical Front and the Subantarctic Front, the Polar Frontal Zone (hereafter PFZ), between the Subantarctic Front and the Polar Front, and the Antarctic Zone (hereafter AZ), south of the Polar Front. Data were principally sourced from the GEOTRACES IDP2017 (Schlitzer et al., 2018) complemented with additional data sets to address data gaps as described below.

Carbon isotopes in dissolved inorganic carbon (DIC) were collected along GEOTRACES sections GA03 (Quay & Wu, 2015) and GP16 (P. Quay, unpublished data available in IDP2017, Schlitzer et al., 2018). Nitrogen isotopes of dissolved nitrate plus nitrite were collected on GEOTRACES section GA03 (Marconi et al., 2015) and GP16 (Peters et al., 2018). As no Southern Ocean DIC or nitrate isotope data are available in GEOTRACES IDP2017, CLIVAR P16S DIC carbon isotopes (Feely et al., 2008, accessed from GLODAPv2.2020, Olsen et al., 2020), and nitrogen isotopes of nitrate plus nitrite (Rafter et al., 2013) were included. Silicon isotopes in dissolved silicic acid were collected along GEOTRACES section GA03 (Brzezinski & Jones, 2015) and GIPY04 (Fripiat et al., 2012).

Available data from each region (typically representing 3–10 hydrographic stations) were fit with a spline in MATLAB (function “smoothingspline”) using a smoothing parameter (p) of 1×10^{-4} to 1×10^{-6} . The exact value of p was chosen to minimize root mean square error and depict regional-scale water column features while diminishing local variability (Figure 3). The spline was then interpolated onto 33 standardized depth intervals following GLODAP mapping protocols (Lauvset et al., 2016).

3. Common Processes

Phytoplankton typically uptake and assimilate elements with a preference for the lighter isotope (Figure 1). The kinetic isotopic effect of assimilation is determined by the ratio of the rates at which each reactant isotope is converted to product:

$$\varepsilon = 1 - \left(\frac{i+n k}{i k} \right) \quad (4)$$

where ε represents the isotope fractionation expressed in ‰ and $i+n k$ and $i k$ are the reaction rates for the reactant bearing the heavy and light isotope, respectively. Observed values of ε in marine phytoplankton are ~19‰ for C (e.g., ¹²C is assimilated over ¹³C by ~19 parts per thousand) (Degens et al., 1968; Sackett et al., 1965), and 4‰–7‰ for N (Fripiat et al., 2019; Waser et al., 1998). Diatoms, the most common autotrophic silicifying organisms, exhibit a similar preference for isotopically lighter dissolved Si by ~1‰ (e.g., De la Rocha et al., 1997; Sutton et al., 2013).

Simple quantitative models relate the isotopic composition of the nutrient (or C) supply and the degree of biological nutrient (or C) utilization to the isotopic composition of biogenic production (Mariotti et al., 1981; Sigman & Fripiat, 2019). Broadly, these models follow closed system (“Rayleigh”) or open system (“steady-state”) pathways:

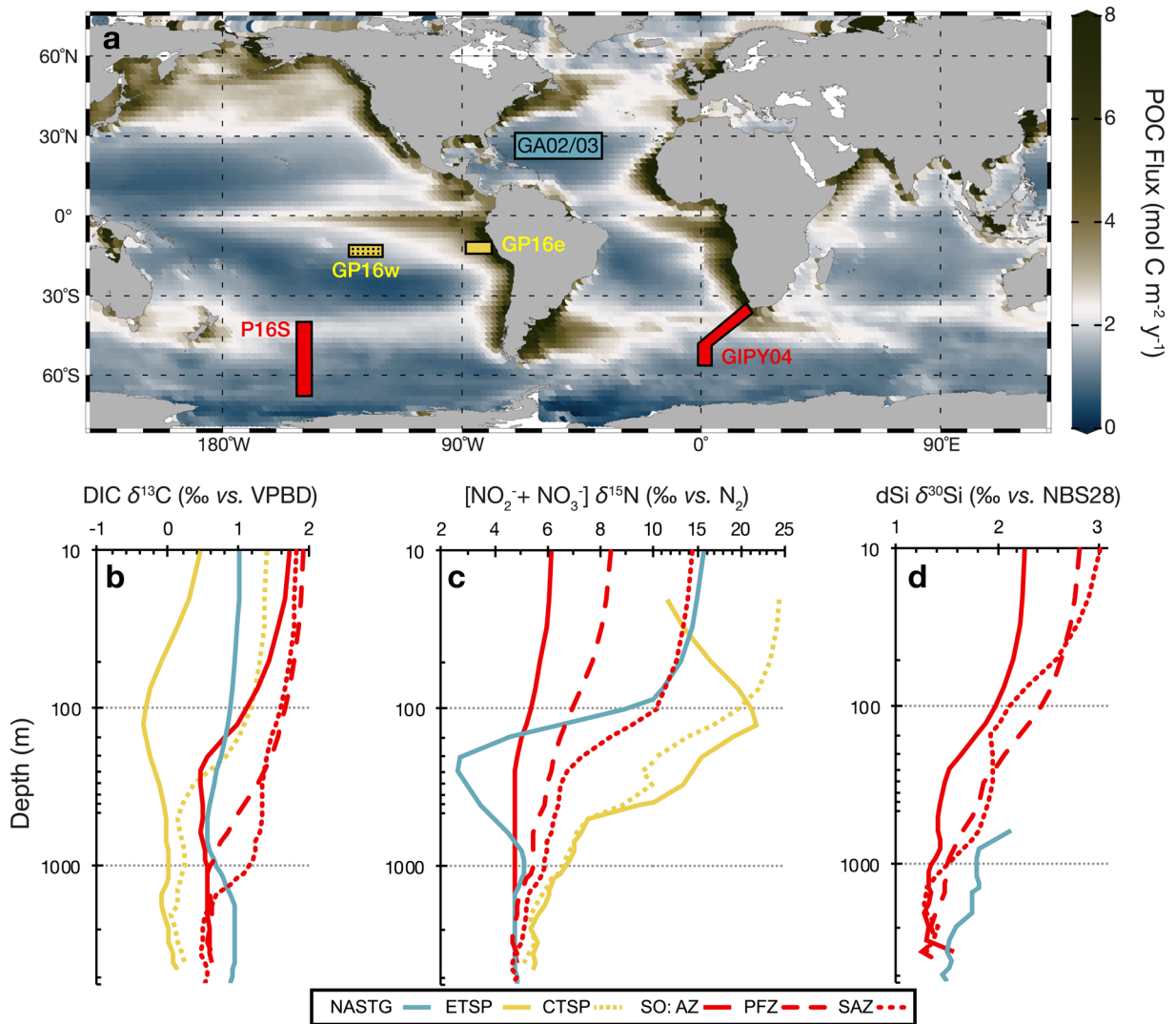


Figure 4. Water column profiles of major element isotope ratios. (a) Global data assimilation model of net export production calculated as C flux at the base of the euphotic zone (DeVries & Weber, 2017). Colored boxes denote regions and cruises of water column element concentration and isotope data. (b) C isotopes in dissolved inorganic carbon (DIC), (c) N isotopes in nitrate + nitrite, (d) Si isotopes in silicic acid versus depth. Lines are smoothed spline fits to water column data (Figure 3). In the Southern Ocean, solid red line indicates data from the southernmost Antarctic Zone (AZ), dashed red line includes data from the Polar Frontal Zone (PFZ), and dotted red line includes data from the northernmost Subantarctic Zone (SAZ). Blue line is from the North Atlantic Subtropical Gyre (NASTG), solid yellow line is from the Eastern Tropical South Pacific (ETSP), and dashed yellow line is from Central Tropical South Pacific (CTSP). See Section 2.2 for data sources.

$$\text{Closed system (Rayleigh)} : \delta^i X_{\text{biogenic}} = \delta^i X_{\text{nutrient supply}} + \epsilon * \left[\frac{f}{(1-f)} \right] * \ln(f) \quad (5)$$

$$\text{Open system (Steady - state)} : \delta^i X_{\text{biogenic}} = \delta^i X_{\text{nutrient supply}} - \epsilon * f \quad (6)$$

where for a given element X, $\delta^i X_{\text{nutrient supply}}$ is the isotopic composition of the nutrient (or carbon) supply, ϵ is the isotopic fractionation during assimilation (Equation 4), and f is the fraction of the nutrient supply used (0–1 or 0%–100%). In the Rayleigh model (Equation 5), the accumulated biogenic production derives from a nutrient pool that is “closed” from resupply or loss (aside from uptake) during biogenic production. In the

steady-state model (Equation 6), the accumulated biogenic production derives from a nutrient pool that is “open” and subject to continuous resupply (hence the pool is neither depleted nor accumulates over time).

The above models and Figure 1 highlight two consequences for C, N, and Si isotopes. First, it is clear that the biological consumption of C, N, and Si, biogenic export, and remineralization (arrows inside orange box, Figure 1) exert a first-order control on the isotopic compositions of exported biogenic production as well as the oceanic dissolved inorganic C, N, and Si inventories. If the isotopic composition of nutrient supply and the kinetic isotope effect during assimilation can be constrained, isotopic measurements in a sediment archive that faithfully records biogenic production could constrain past *nutrient utilization* using Equations 5 and 6.

However, the second consequence arises from the above assumptions and the simplicity of Equations 5 and 6. It is equally clear from Figure 1 that other processes—both internal and at interfaces—can alter the isotopic composition of nutrient supply (arrows outside orange box). Furthermore, a change in the concentration of the nutrient supply, for instance due to a change in physical circulation, makes interpretation of nutrient utilization difficult using these simple models (e.g., Kemeny et al., 2018). Uncertainty in the concentration and isotopic composition of the combined nutrient source in Equations 5 and 6 poses both a challenge and an opportunity. The challenge is that these assumptions must be addressed with significant additional constraints if C, N, or Si isotopes are to quantitatively track C or nutrient utilization. The opportunity is that, even when these assumptions do not hold, C, N, and Si isotopes can still provide valuable information on processes impacting C and nutrient inputs to and losses from the ocean.

4. Carbon Isotopes

Dissolved inorganic carbon (DIC) is present in abundant quantities in the oceans as aqueous carbon dioxide (CO_2), bicarbonate (HCO_3^-), and carbonate ion (CO_3^{2-}). As C is an essential element for life, biological production consumes DIC. However, DIC consumption differs from that of dissolved N and Si in one key fashion. Whereas N and Si are principally supplied from the ocean interior and may be completely consumed in surface waters (i.e., *limiting nutrients*, Sections 5 and 6), DIC is never completely consumed in the surface ocean, reflecting both its abundant concentration and continual resupply by exchange with atmospheric CO_2 (Figure 1).

Deviations in the abundances of the two stable C isotopes (^{12}C and ^{13}C) throughout the water column reflect a combination of biological, physical, and chemical processes. Here, we focus on the $\delta^{13}\text{C}$ of DIC ($\delta^{13}\text{C}_{\text{DIC}}$), which primarily reflects the $\delta^{13}\text{C}$ of bicarbonate because the DIC pool is >90% bicarbonate at the average ocean pH of 8.1.

4.1. Modern Ocean $\delta^{13}\text{C}_{\text{DIC}}$ Distribution

The general pattern of $\delta^{13}\text{C}_{\text{DIC}}$ in the modern ocean consists of higher $\delta^{13}\text{C}_{\text{DIC}}$ in the surface ocean, a subsurface minimum between 100 and 1,000 m depth, and lower $\delta^{13}\text{C}_{\text{DIC}}$ in deeper waters (Figure 4b). The highest $\delta^{13}\text{C}_{\text{DIC}}$ occurs in the upper 100 m of the SO SAZ, PFZ, and AZ, and the lowest $\delta^{13}\text{C}_{\text{DIC}}$ overall occurs in the ETSP. The difference in surface ocean $\delta^{13}\text{C}_{\text{DIC}}$ between these regions is $\sim 1.5\text{‰}$. Below 1,000 m, $\delta^{13}\text{C}_{\text{DIC}}$ is highest in the NASTG, followed by the SO, and lowest in the ETSP and CTSP, with a range of $\sim 1\text{‰}$. Of the regions shown in Figure 4b, the NASTG has the lowest gradient of $\delta^{13}\text{C}_{\text{DIC}}$ with depth. While the ETSP, CTSP, and SO all have lower $\delta^{13}\text{C}_{\text{DIC}}$ below 1,000 m than in the upper 10 m, the NASTG has similar $\delta^{13}\text{C}_{\text{DIC}}$ values in the upper 10 m and below 1,000 m. The regional contrast in these patterns is due to spatial differences in the strength of driving processes and varying oceanographic regimes, as described next.

4.2. Driving Processes of Modern Ocean $\delta^{13}\text{C}_{\text{DIC}}$ Distribution

Analyzing the distribution of $\delta^{13}\text{C}_{\text{DIC}}$ in the global oceans, Kroopnick (1974, 1985) noted that $\delta^{13}\text{C}_{\text{DIC}}$ was mainly influenced by photosynthetic kinetic fractionation and respiration in the surface waters and remineralization of organic matter via microbial respiration in the deeper ocean. Marine phytoplankton preferentially incorporate the lighter ^{12}C during photosynthesis, leaving the photic zone DIC relatively more

enriched in ^{13}C (Figure 1). This fractionation of $\sim 19\%$ for marine photosynthesis leaves the residual DIC in the nutrient depleted surface ocean with high $\delta^{13}\text{C}_{\text{DIC}}$ compared to that of deep water (Lynch-Stieglitz et al., 1995). As organic matter, which is enriched in ^{12}C , sinks out of the photic zone, it is subject to microbial degradation and remineralization. This process results in the release of ^{12}C enriched DIC and nutrients at depth, lowering the $\delta^{13}\text{C}_{\text{DIC}}$ of deeper waters. A decreasing trend in the production of organic matter in the photic zone will decrease $\delta^{13}\text{C}_{\text{DIC}}$ in the surface ocean and increase $\delta^{13}\text{C}_{\text{DIC}}$ at depth, as less ^{12}C is removed from the DIC pool for photosynthesis and released at depth during remineralization (Figure 1).

A further feature of the $\delta^{13}\text{C}_{\text{DIC}}$ of deep water is the gradual increase in ^{12}C enrichment with time as a result of accumulated organic matter respiration at depth, beginning at the time a water mass is no longer in contact with the atmosphere. As a result, the $\delta^{13}\text{C}_{\text{DIC}}$ of deep waters decreases with the increasing age of the water mass. Following the broad pattern of global deep ocean circulation, this effect results in lower $\delta^{13}\text{C}_{\text{DIC}}$ in the deep Pacific than in the deep Atlantic at present (Figure 4b) and makes $\delta^{13}\text{C}$ a nonconservative tracer of deep-water masses (e.g., Curry & Oppo, 2005).

In addition to biological $\delta^{13}\text{C}$ fractionation, equilibrium fractionation during air-sea gas exchange can influence the $\delta^{13}\text{C}_{\text{DIC}}$ in surface seawater (Figure 1). If atmospheric CO_2 were in isotopic equilibrium with oceanic DIC, the DIC pool would be enriched in ^{13}C relative to atmospheric CO_2 by $\sim 8\%$ at 20°C (Zhang et al. 1995). During dissolution of atmospheric CO_2 into surface seawater, aqueous CO_2 fractionates by -1.1% at 20°C , but subsequent fractionation during carbonic acid dissociation to HCO_3^- and CO_3^{2-} results in an overall enrichment of $\sim 8\%$ (Lynch-Stieglitz et al. 1995). These equilibrium fractionations also depend on the temperature of equilibration, with surface water DIC becoming more enriched relative to atmospheric CO_2 by $\sim 1\%$ per degree of cooling (Mook et al., 1974). However, for a 50 m deep surface mixed layer, it would take ~ 10 years for the C isotopes to equilibrate between the atmosphere and ocean, which is longer than the residence time of most water masses at the ocean surface (Broecker & Peng, 1982). The timescale for this equilibration also varies as a function of atmospheric $p\text{CO}_2$, with higher $p\text{CO}_2$ leading to a faster isotopic equilibration between surface ocean DIC and atmospheric CO_2 (Galbraith et al., 2015). As a result, there is no region in the ocean today where surface water $\delta^{13}\text{C}_{\text{DIC}}$ is in complete isotopic equilibrium with atmospheric $\delta^{13}\text{C}_{\text{CO}_2}$ (Broecker & Maier-Reimer, 1992), and the degree of equilibration has certainly changed in the past under different $p\text{CO}_2$ levels (Galbraith et al., 2015). In some regions, the effects of gas exchange and biology on surface water $\delta^{13}\text{C}_{\text{DIC}}$ work together, such as in the subpolar oceans where both tend to increase $\delta^{13}\text{C}_{\text{DIC}}$, while in the subtropics, biology acts to increase $\delta^{13}\text{C}_{\text{DIC}}$ but gas exchange tends to decrease $\delta^{13}\text{C}_{\text{DIC}}$ (Schmittner et al., 2013) (Figures 1 and 4b).

Another factor that has influenced oceanic $\delta^{13}\text{C}_{\text{DIC}}$ over the industrial era is the ^{13}C “Suess” effect (Keeling, 1979). The CO_2 emitted to the atmosphere from fossil fuel combustion is strongly depleted in ^{13}C , leading to a reduction in the $\delta^{13}\text{C}$ of atmospheric CO_2 . Measurements from air trapped in ice cores show that the preindustrial background $\delta^{13}\text{C}_{\text{CO}_2}$ was around -6.4% (Bauska et al., 2015), but had declined to -8.4% by 2014 (Keeling et al., 2017). Air-sea exchange has resulted in the propagation of this Suess effect into the upper ocean, decreasing upper ocean $\delta^{13}\text{C}_{\text{DIC}}$ values (Eide et al., 2017) and reducing the $\delta^{13}\text{C}_{\text{DIC}}$ gradient between the surface and deep ocean (Olsen & Ninnemann, 2010).

4.3. $\delta^{13}\text{C}$ Archives

Planktic and benthic foraminifera are the most commonly used archives for reconstructing past $\delta^{13}\text{C}_{\text{DIC}}$ because the $\delta^{13}\text{C}$ of their CaCO_3 test is controlled by the $\delta^{13}\text{C}_{\text{DIC}}$ of the seawater in which the test precipitated. The use of foraminiferal $\delta^{13}\text{C}$ as a C cycle proxy was first suggested by Tappan (1968), who noted that higher $\delta^{13}\text{C}$ values in the carbonate tests of surface-dwelling planktic foraminifera were indicative of periods of increased organic C burial in marine sediments and possibly increased NEP. However, laboratory experiments have also demonstrated that the $\delta^{13}\text{C}$ of planktic foraminiferal calcite varies with symbiont photosynthesis, respiration, and seawater $[\text{CO}_3^{2-}]$ (Spero, 1998). The combined influence of these physiological processes shifts planktic foraminiferal $\delta^{13}\text{C}$ away from C isotopic equilibrium. C isotope data obtained from tests collected from plankton tows or sediment traps can help determine average population or even specific species offsets from $\delta^{13}\text{C}_{\text{DIC}}$ so that the fossil record of planktic foraminiferal $\delta^{13}\text{C}$ can be used to reconstruct past $\delta^{13}\text{C}_{\text{DIC}}$ (Spero et al., 2003). The $\delta^{13}\text{C}$ of epifaunal benthic foraminifera species that live close to the sedi-

ment/water interface generally reflects the $\delta^{13}\text{C}_{\text{DIC}}$ of bottom water masses and can be used to reconstruct the $\delta^{13}\text{C}_{\text{DIC}}$ of deep waters (Woodruff et al., 1980).

The $\delta^{13}\text{C}$ difference between surface-dwelling planktic and epifaunal benthic foraminifera can be used to reconstruct the vertical gradients in $\delta^{13}\text{C}_{\text{DIC}}$ between the surface and deep ocean in the past. Theoretically, these vertical gradients should reflect the integrated efficiency of the ocean's biological pump (Broecker, 1982; Shackleton et al., 1983), with a larger difference between planktic and benthic $\delta^{13}\text{C}$ (e.g., a steeper $\delta^{13}\text{C}_{\text{DIC}}$ gradient) indicating a more efficient biological pump for the time period of interest. However, this approach is subject to significant caveats because the bottom water $\delta^{13}\text{C}_{\text{DIC}}$ signal is integrated over space and time (Section 4.4 below). Because export productivity varies considerably in the ocean at any given time, samples from many sites need to be analyzed to obtain a meaningful global average.

Another use of foraminifera $\delta^{13}\text{C}$ relies on $\delta^{13}\text{C}$ gradients between bottom waters and sediments. While the $\delta^{13}\text{C}$ of epifaunal benthic foraminifera reflects the $\delta^{13}\text{C}_{\text{DIC}}$ of bottom water, infaunal species that calcify within the sediment pore water record a $\delta^{13}\text{C}_{\text{DIC}}$ signal dependent on bottom-water dissolved oxygen contents and organic matter fluxes (McCorkle et al., 1990). The $\delta^{13}\text{C}$ difference between epifaunal and shallow infaunal benthic foraminiferal $\delta^{13}\text{C}$ values ($\Delta\delta^{13}\text{C}_{\text{E-I}}$) has been suggested as a proxy for bottom water oxygen concentration, which may relate to export production given that the $\delta^{13}\text{C}$ difference is proportional to the organic C flux to the seafloor and related remineralization rate of organic matter in the uppermost sediment layer (Hoogakker et al., 2015, 2018; McCorkle et al., 1990).

4.4. Sources of Uncertainty

Using $\delta^{13}\text{C}$ to quantify past C cycling is not straightforward because, as noted above, changes in ocean circulation, air-sea equilibration, gas exchange, upwelling, and mixing of water masses can also modify $\delta^{13}\text{C}_{\text{DIC}}$, and thus foraminiferal $\delta^{13}\text{C}$, independent of changes in export production. These uncertainties can be framed in terms of preformed and regenerated C (Box 1). In the ideal case, deep ocean $\delta^{13}\text{C}_{\text{DIC}}$ would only reflect regenerated carbon derived from export production in the overlying water column at a given location. In reality, the deep water $\delta^{13}\text{C}_{\text{DIC}}$ at a given location integrates locally regenerated C, the regenerated C inventory accumulated along the transit history of the deep ocean water mass, and the preformed C contribution from when the water mass was last in contact with the atmosphere. These two non-local contributions also include the effects of air-sea equilibration and gas exchange from when that parcel of water was last at the surface and from mixing and water mass aging as the water transits the ocean's interior. Furthermore, reconstructions over time from a single location cannot discriminate between $\delta^{13}\text{C}_{\text{DIC}}$ changes due to internal processes (export production, air-sea exchange, and circulation) and external processes (e.g., C input from the terrestrial biosphere).

Studies using foraminiferal $\delta^{13}\text{C}$ gradients address potential overlaps from external processes, as any mean ocean $\delta^{13}\text{C}_{\text{DIC}}$ change should affect all records equally. However, consideration must be given to how internal processes might affect each foraminiferal $\delta^{13}\text{C}$ record. For instance, in studies using $\delta^{13}\text{C}$ gradients between the surface and deep ocean using planktic and benthic foraminifera, the effects of air-sea equilibration, gas exchange, upwelling, and mixing need to be considered near the sea surface for planktic foraminifera $\delta^{13}\text{C}$ as well as in bottom waters for benthic foraminifera $\delta^{13}\text{C}$.

Other uncertainties relate to the correlation between foraminiferal $\delta^{13}\text{C}$ and $\delta^{13}\text{C}_{\text{DIC}}$. These include species-specific fractionations (Spero et al., 2003) and the influence of seawater $[\text{CO}_3^{2-}]$ on foraminiferal $\delta^{13}\text{C}$ (Spero et al., 1997). For reconstructions based on epifaunal-infaunal benthic $\delta^{13}\text{C}$ differences ($\Delta\delta^{13}\text{C}_{\text{E-I}}$), regeneration of organic matter in sediment depends on the oxygenation of deep water, which is also a function of circulation and temperature. The $\delta^{13}\text{C}$ of infaunal foraminifera may also be modified by contributions of isotopically light C from anaerobic processes (denitrification and sulfate reduction) in sediment pore waters, which can bias oxygenation reconstructions based on the $\Delta\delta^{13}\text{C}_{\text{E-I}}$ proxy (Jacobel et al., 2020).

These uncertainties might seem to paint a pessimistic view of the utility of $\delta^{13}\text{C}$ proxies relative to the $\delta^{15}\text{N}$ and $\delta^{30}\text{Si}$ tools discussed below. In reality, this reflects the longevity of foraminifera $\delta^{13}\text{C}$ relative to other proxies. With over 50 years of study, there is detailed knowledge of the $\delta^{13}\text{C}$ proxy and thus its limitations. Furthermore, unlike for other nutrient isotope proxies, there is a wealth of published paleo- $\delta^{13}\text{C}$ records to

facilitate modeling efforts (e.g., Schmittner & Lund, 2015). Applications of C isotopes to understand past C and nutrient cycling and opportunities for future research are discussed further in Section 7.

5. Nitrogen Isotopes

Bioavailable N (“fixed” from atmospheric N_2) in the ocean exists predominantly as nitrate (NO_3^-), with smaller but locally important contributions of ammonium (NH_4^+) and nitrite (NO_2^-). The supply of NO_3^- limits biological productivity in much of the tropical and temperate oceans (Moore et al., 2013). Indeed, the quantity of organic matter exported from the surface ocean (e.g., NEP) has been linked directly to NO_3^- consumption (Dugdale & Goering, 1967; Eppley & Peterson, 1979). Input and loss fluxes of fixed N are large relative to the oceanic fixed N inventory, with fixed N having an estimated residence time of less than 3,000 years (Brandes & Devol, 2002; Somes et al., 2013). Given the ubiquitous demand for fixed N by primary producers, N and its stable isotopes (^{15}N and ^{14}N) trace the degree of NO_3^- consumption for certain oceanographic settings and can inform on changes in marine fixed N sources and sinks in other settings.

The formalized relationship between marine nitrate $\delta^{15}N$ and the $\delta^{15}N$ of organic matter (and therefore all $\delta^{15}N$ proxies) in Equations 5 and 6 highlights two key processes to consider when interpreting paleoceanographic $\delta^{15}N$ records: (a) the $\delta^{15}N$ value of the initial NO_3^- (the “nutrient supply”) upwelled to the surface and (b) the degree of NO_3^- utilization (f). Below, we examine the marine biogeochemical processes that influence the initial NO_3^- $\delta^{15}N$.

5.1. Modern Ocean Nitrate $\delta^{15}N$ Distribution

The $\delta^{15}N$ of NO_3^- (hereafter $\delta^{15}N_{\text{nitrate}}$) broadly decreases from the surface to deep ocean in all regions (Figure 4c). The highest $\delta^{15}N_{\text{nitrate}}$ is observed in the upper 50 m of the CTSP and NASTG, with progressively lower $\delta^{15}N_{\text{nitrate}}$ in the upper 50 m of the SAZ, PFZ, and AZ, respectively. In the ETSP oxygen-deficient zone, $\delta^{15}N_{\text{nitrate}}$ increases with depth to a maximum around 120 m before progressively decreasing below 120 m. A sharp $\delta^{15}N_{\text{nitrate}}$ decrease with depth between 40 and 300 m is observed in low latitude regions. At these depths, NASTG $\delta^{15}N_{\text{nitrate}}$ is notably lower ($<4\%$), while ETSP and CTSP $\delta^{15}N_{\text{nitrate}}$ are higher ($>8\%$) than Southern Ocean $\delta^{15}N_{\text{nitrate}}$ (5% – 7%). At depths below 3,000 m, $\delta^{15}N_{\text{nitrate}}$ from all major ocean basins converges on the mean deep ocean value of $5.0 \pm 0.3\%$ (Rafter et al., 2019; Sigman et al., 2000).

5.2. Driving Processes

First, if NO_3^- is not completely consumed at the surface ($f > 0$), phytoplankton will preferentially incorporate $^{14}NO_3^-$ (Altabet & Francois, 1994). As NO_3^- utilization increases, this preferential $^{14}NO_3^-$ consumption progressively elevates the residual $\delta^{15}N_{\text{nitrate}}$ in the surface ocean relative to the subsurface NO_3^- supply. This fractionation during uptake explains the elevated ($>10\%$) $\delta^{15}N_{\text{nitrate}}$ in the upper ~ 100 m of the NASTG relative to the subsurface NO_3^- source (Figure 4c; Marconi et al., 2015). In the upper 100 m of the CTSP, residual NO_3^- is isotopically elevated to $>20\%$; these high values represent near-complete biological NO_3^- consumption of a subsurface NO_3^- source that is much higher in $\delta^{15}N$ than in the NASTG (Peters et al., 2018), for reasons discussed below. In the upper 100 m of the Southern Ocean, $\delta^{15}N_{\text{nitrate}}$ increases from south to north, with the lowest $\delta^{15}N_{\text{nitrate}}$ observed close to the location of deep water upwelling in the AZ. As these surface waters move equatorward, increasing fractional NO_3^- utilization leads to higher $\delta^{15}N_{\text{nitrate}}$ in residual NO_3^- present in the surface PFZ and SAZ, respectively.

Below the euphotic zone (“subsurface” or $\sim >100$ m), $\delta^{15}N_{\text{nitrate}}$ is primarily controlled by organic matter regeneration and the associated nitrification of organic N to NO_3^- , external pathways of fixed N gain/loss, and transport of preformed and regenerated NO_3^- . For example, while N_2 fixation occurs within the euphotic zone, this process is observable in subsurface waters via regeneration of organic matter with a low $\delta^{15}N$ of $\sim -1\%$ (Carpenter et al., 1997; Hoering & Ford, 1960; Knapp et al., 2008). For many ocean regions, organic matter regeneration effectively exports surface ocean $\delta^{15}N_{\text{nitrate}}$ values to the deep sea and thus impacts ambient subsurface $\delta^{15}N_{\text{nitrate}}$ (Casciotti et al., 2008; Rafter et al. 2013; Sigman et al. 2009). Within the subsurface ocean, fixed N (and NO_3^-) is removed from the ocean via water column denitrification, which preferentially removes ^{14}N in oxygen-deficient zones, leaving the residual NO_3^- enriched in ^{15}N (Cline &

Kaplan, 1975). It is important to note that because denitrification reduces the NO_3^- inventory, in the context of an isotopic mass-balance, increased denitrification actually diminishes the influence of this newly elevated $\delta^{15}\text{N}_{\text{nitrate}}$ on NO_3^- outside of the denitrification area (Deutsch et al., 2004). In the deep sea (below 3,000 m), small ($\sim 0.5\%$) inter-basin differences in $\delta^{15}\text{N}_{\text{nitrate}}$ may reflect the regional regeneration of organic matter with different $\delta^{15}\text{N}$ (Rafter et al., 2019).

Because of additional controls on N_2 fixation and water column denitrification, these processes are not co-located within the oceans (Figure 1), resulting in significant regional $\delta^{15}\text{N}_{\text{nitrate}}$ deviations. Specifically, the regional dominance of N_2 fixation lowers subsurface $\delta^{15}\text{N}_{\text{nitrate}}$ in the NASTG (Marconi et al., 2015), while water column denitrification raises subsurface $\delta^{15}\text{N}_{\text{nitrate}}$ in the ETSP (Peters et al., 2018) (Figure 4c). Benthic denitrification has a weak isotope effect relative to water column denitrification (Brandes & Devol, 2002; Lehmann et al., 2007), but it likely has an important indirect effect by stimulating additional N_2 fixation that delivers low $\delta^{15}\text{N}_{\text{nitrate}}$ to the ocean (Ren et al., 2017; Somes et al., 2013).

Given the pronounced regional disparity of the three processes described (fractional NO_3^- utilization, N_2 fixation, and denitrification), one might expect that their impact on subsurface $\delta^{15}\text{N}_{\text{nitrate}}$ would be limited to regions where these processes actively occur. However, both ocean circulation and the export and remineralization of sinking organic matter work to transfer the isotopic signatures of these processes outside of the regions of their activity. For example, the sinking of surface Southern Ocean waters that experienced partial NO_3^- assimilation leads to high preformed $\delta^{15}\text{N}_{\text{nitrate}}$ in thermocline and intermediate waters (Rafter et al., 2012, 2013; Tuerena et al., 2015). This signature can be traced into the North Atlantic (Marconi et al., 2015); note the similar $\delta^{15}\text{N}_{\text{nitrate}}$ at 1,000 m in the SAZ, PFZ and NASTG (Figure 4c). Additionally, the assimilation of high $\delta^{15}\text{N}_{\text{nitrate}}$ in surface waters overlying oxygen-deficient zones leads to high $\delta^{15}\text{N}$ in sinking organic matter, which is then regenerated to high subsurface $\delta^{15}\text{N}_{\text{nitrate}}$. Multiple cycles of assimilation/regeneration and upper ocean circulation allow for spreading of the high subsurface $\delta^{15}\text{N}_{\text{nitrate}}$ signature from within oxygen-deficient zones (ETSP) to areas where water column denitrification does not actively occur (CTSP) (Figure 4c; Peters et al., 2018; Sigman et al., 2009).

To summarize, the isotopic fractionations associated with the following processes act to determine marine $\delta^{15}\text{N}_{\text{nitrate}}$ (Figure 1): (a) partial NO_3^- utilization, which elevates surface ocean $\delta^{15}\text{N}_{\text{nitrate}}$ as well as global thermocline $\delta^{15}\text{N}_{\text{nitrate}}$ via mode and intermediate waters (Marconi et al., 2015; Rafter et al. 2012, 2013), (b) N_2 fixation, which lowers marine $\delta^{15}\text{N}_{\text{nitrate}}$ via remineralization of organic matter, and (c) water column denitrification, which locally elevates the residual $\delta^{15}\text{N}_{\text{nitrate}}$ (e.g., Rafter et al., 2019; Sigman & Fripiat, 2019; Somes et al., 2010).

5.3. $\delta^{15}\text{N}$ Archives

There is a clear, observable link between surface ocean $\delta^{15}\text{N}_{\text{nitrate}}$, the degree of NO_3^- utilization, and sinking organic matter $\delta^{15}\text{N}$ (Fawcett et al., 2011). As can be seen in Equations 5 and 6, the main influences on sinking organic matter $\delta^{15}\text{N}$ are the initial $\delta^{15}\text{N}_{\text{nitrate}}$ and the degree of surface NO_3^- utilization. For example, in oligotrophic waters where NO_3^- consumption is complete ($f \sim 0$; see Equations 5 and 6), the upwelled $\delta^{15}\text{N}_{\text{nitrate}}$ (the “initial $\delta^{15}\text{N}_{\text{nitrate}}$ ”) should equal the sinking organic matter $\delta^{15}\text{N}$ due to mass balance (Equations 5 and 6). Conversely, in eutrophic waters where there is incomplete nitrate utilization ($f > 0$, Equations 5 and 6), sinking organic matter $\delta^{15}\text{N}$ is informed by both the initial $\delta^{15}\text{N}_{\text{nitrate}}$ (establishing the upper bound) and the degree of NO_3^- utilization (Equations 5 and 6).

Bulk sediments are an attractive archive for reconstructing past sinking organic matter $\delta^{15}\text{N}$ given the relative ease of measurement via elemental analyzer-isotope ratio mass spectrometry. While there is evidence that bulk sediment $\delta^{15}\text{N}$ accurately records surface water processes in continental margin sediments and high accumulation rate areas (Robinson et al., 2012), bulk sediment $\delta^{15}\text{N}$ may be modified from sinking $\delta^{15}\text{N}$ by microbial degradation in the water column (e.g., Gaye et al., 2013; Gaye-Haake et al., 2005), after deposition on the seafloor (Freudenthal et al., 2001; Möbius et al., 2011), and by addition of non-marine organic matter (Robinson et al., 2012; Schubert & Calvert, 2001).

In response to this potentially, and in some cases demonstrably altered or contaminated bulk sediment organic matter $\delta^{15}\text{N}$ archive (M. Kienast et al., 2005; Martínez-García et al., 2014; Ren et al., 2009; Robinson

et al., 2012; Straub et al., 2013), several new proxy methods have been developed to isolate sinking organic N in the sediments. One approach examines the $\delta^{15}\text{N}$ of specific organic compounds either derived (amino acids, McCarthy et al., 2013) or degraded from surface ocean productivity (geoporphyrins from chlorophyll degradation, Higgins et al., 2009). Another approach measures the $\delta^{15}\text{N}$ on organic matter bound within biominerals produced in the upper ocean (e.g., diatoms, radiolaria, and planktic foraminifera, Horn, Robinson, et al., 2011; Martínez-García et al., 2014; Ren et al., 2009, 2012; Robinson et al., 2005, 2015; Sigman et al., 1999; Smart et al., 2018, 2020; Studer et al., 2015), and on biominerals produced in the deep ocean (deep-sea corals that feed on sinking organic matter, Wang et al., 2014, 2017). These archives are certainly less prone to bias from allochthonous N input and are presumably more resistant to diagenetic N isotope fractionation. For example, even though there is loss of bound N between foraminifera collected in net tows, sediment traps, and in sediments, only minor isotopic fractionation is observed (Smart et al., 2018, 2020). However, the compound-specific and fossil-bound $\delta^{15}\text{N}$ methods for reconstructing sinking organic matter $\delta^{15}\text{N}$ also come with their own complexities, including more intensive preparatory chemistry, sample limitation, and potential differences in species' internal N cycling for fossil-bound approaches (e.g., LeKieffre et al., 2020; Smart et al., 2018).

5.4. Sources of Uncertainty in Reconstructions of Past NO_3^- Utilization

The Rayleigh and steady-state models (Equations 5 and 6) provide a useful framework for assessing sources of uncertainty in reconstructions of past NO_3^- utilization from $\delta^{15}\text{N}$ measurements in sedimentary archives. First, considering the left side of these equations, there is uncertainty in the biogenic production tracked by the $\delta^{15}\text{N}$ of sediment archives. Here an ideal archive would track the sinking organic matter $\delta^{15}\text{N}$, as this is directly related to the new NO_3^- supply to the surface ocean (Fawcett et al., 2011). However, with regard to fossil-bound N isotopes at high latitudes, diatoms (phytoplankton) and foraminifera (zooplankton) dominate euphotic zone biological production at different times in the seasonal bloom. Their respective N isotope signatures may be “snapshots” of the N isotopic composition of surface ocean organic matter production at different times, requiring consideration of the appropriate Rayleigh model for interpretation (e.g., instantaneous vs. integrated production models; Ren et al., 2015). Seasonality also manifests in the observation that foraminifera may consume particulate organic N derived from recycled N during parts of the growing season (Smart et al., 2018, 2020). However, it is unclear whether this seasonal decoupling of fossil-bound $\delta^{15}\text{N}$ from the $\delta^{15}\text{N}$ of newly supplied NO_3^- could be maintained in the flux of foraminifera to sediments (Smart et al., 2018, 2020). Finally, there are logistical hurdles in these measurements, including the separation of individual diatom species (Studer et al., 2015) and diatoms from other silicifiers, which may have starkly different $\delta^{15}\text{N}$ (Ren et al., 2015; Robinson et al., 2015). Further study of fossil-bound N isotopes will help address these issues.

Next, considering the right side of the Rayleigh and steady-state models (Equations 5 and 6), a large source of uncertainty lies in constraining the initial supply NO_3^- concentration and $\delta^{15}\text{N}_{\text{nitrate}}$. There are currently no proxies for subsurface $\delta^{15}\text{N}_{\text{nitrate}}$ outside of oligotrophic areas where surface NO_3^- is completely consumed and the sinking organic matter $\delta^{15}\text{N}$ will represent $\delta^{15}\text{N}$ of NO_3^- supply, or any proxies of deep ocean $\delta^{15}\text{N}_{\text{nitrate}}$. This reflects the dominance of biologically fixed N assimilation in the surface ocean; even deep-sea corals appear to acquire their N from sinking organic N that ultimately derives from the euphotic zone (Wang et al., 2014). To address this, authors have used multiple sediment $\delta^{15}\text{N}$ records to quantify both the source $\delta^{15}\text{N}_{\text{nitrate}}$ signal and the mixed isotopic signal, with varying degrees of success (Galbraith et al., 2008; Rafter & Charles, 2012; Robinson et al., 2009). Models with ^{15}N implemented as a tracer can estimate changes to N cycling on the local and global scale and provide another approach for separating source from utilization isotopic signatures on sediment $\delta^{15}\text{N}$ (Eugster et al., 2013; Galbraith et al., 2013; Somes et al., 2017).

Finally, while the Rayleigh and steady-state models (Equations 5 and 6) have motivated our discussion so far, in some settings these may be too simplified to robustly quantify changes in NO_3^- utilization from sediment $\delta^{15}\text{N}$. In particular, these models consider only a single dimension of vertical NO_3^- resupply from a subsurface NO_3^- reservoir of known concentration and composition that is independent of surface ocean utilization. This oversimplifies fixed N cycling in the Antarctic Zone of the Southern Ocean, where the subsurface NO_3^- concentration and $\delta^{15}\text{N}_{\text{nitrate}}$ is dependent on the degree of NO_3^- utilization in the previous year(s) (Kemeny et al., 2018). Furthermore, the expected relationship between increasing NO_3^- utiliza-

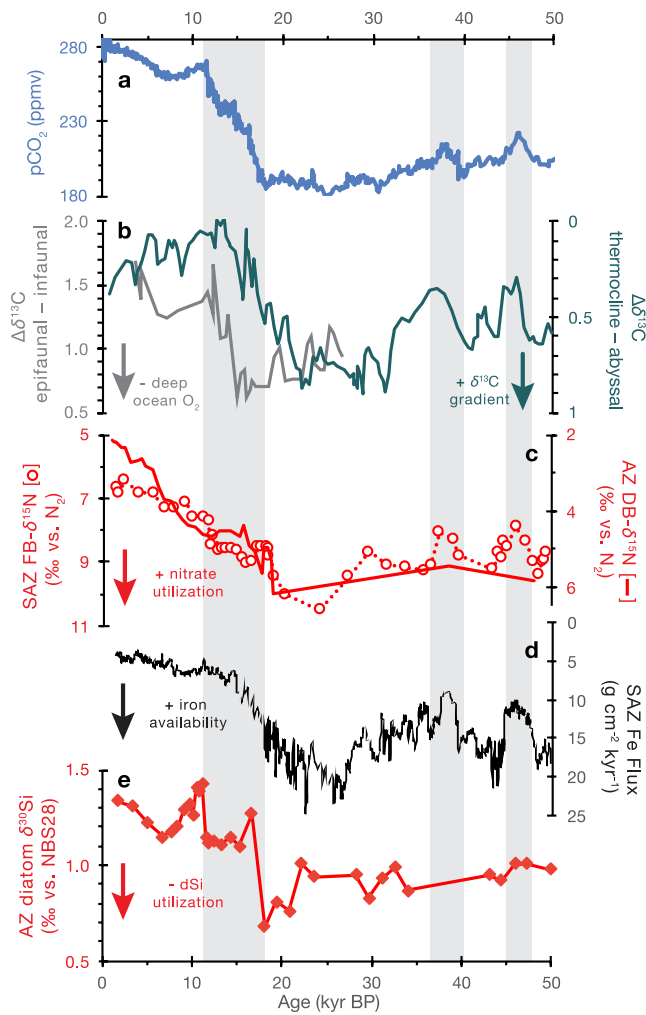


Figure 5. Selected C, N, and Si isotope records across the last glacial cycle. (a) Atmospheric $p\text{CO}_2$ (Antarctic compilation from Ahn & Brook, 2014; Bereiter et al., 2012; MacFarling Meure et al., 2006; Marcott et al., 2014; Monnin et al., 2004; Rubino et al., 2013). (b) $\delta^{13}\text{C}$ gradients between epifaunal and infaunal benthic foraminifera (gray, left axis; Hoogakker et al., 2018) and between intermediate-dwelling planktic and benthic foraminifera (teal, right axis; Ziegler et al., 2013). (c) SAZ foraminifera-bound $\delta^{15}\text{N}$ (circles and dotted line, Martínez-García et al., 2014) and AZ diatom-bound $\delta^{15}\text{N}$ (Studer et al., 2015) indicating Southern Ocean nitrate utilization; note that lower values are plotted upward. (d) Iron flux to the SAZ (Martínez-García et al., 2014). (e) Diatom $\delta^{30}\text{Si}$ indicating AZ dSi utilization (Robinson et al., 2014). Axes in (b–d) are oriented with up/down indicating a process change that is associated with a less/more efficient biological pump. Vertical gray shading highlights three periods of increasing and/or elevated $p\text{CO}_2$: the deglaciation (18.1–11.1 ka), AIM 8 (38 ka), and AIM 12 (47 ka).

tion and increasing $\delta^{15}\text{N}_{\text{nitrate}}$ is distorted in some areas of active N_2 fixation (Casciotti et al., 2008; Somes et al., 2010). The further integration of physical and biogeochemical components in models of NO_3^- utilization is important not only for quantifying how NO_3^- utilization has changed, but also for understanding the mechanisms behind past changes in NO_3^- utilization.

6. Silicon Isotopes

Dissolved silicon (dSi, principally in the form of orthosilicic acid) is an essential nutrient for the large number of marine organisms, known as silicifiers, that produce biogenic silica (bSi) for their skeletal/architectural structures. Silicon is present as three stable isotopes: ^{28}Si , ^{29}Si , and ^{30}Si , and deviations in the natural abundance ratios of these isotopes can reveal information regarding the chemical and biological processes active within oceanic systems (Sutton et al., 2018).

6.1. Modern Ocean dSi and $\delta^{30}\text{Si}$ of dSi Distribution

The global mean dissolved silicon isotopic composition (denoted by $\delta^{30}\text{Si}$) of modern seawater depends on the flux and isotopic composition of the known inputs—rivers and glaciers, groundwater, hydrothermal activity, sedimentary processes, and atmospheric dust—and outputs, namely reverse weathering and burial of bSi (Sutton et al., 2018). Changes in the mass balance of the different inputs, and end-member compositions of the constituents, are likely to cause changes in the budget of dSi and $\delta^{30}\text{Si}$ in the oceans through time, especially over timescales longer than the residence time of silicon in the oceans (~12 ka; Frings et al., 2016). The geographical variation in dSi and $\delta^{30}\text{Si}$ in modern oceanic waters is largely driven by biological uptake and remineralization of bSi, as well as large-scale oceanic circulation and mesoscale mixing processes. As with nitrogen isotopes, $\delta^{30}\text{Si}$ of dSi in surface Southern Ocean waters increases from the AZ to the PFZ and the SAZ (Figure 4d). This reflects preferential incorporation of isotopically light dSi into bSi and resultant isotopic enrichment of the remaining dSi in surface waters, with an increase in relative utilization from the AZ to the PFZ and SAZ (Cardinal et al., 2005; Fripiat et al., 2012). NASTG dSi $\delta^{30}\text{Si}$ is elevated at depth over the Southern Ocean (Figure 4d), indicating the influence of overturning circulation on propagating isotopically enriched dSi from the Arctic Ocean and preformed isotopically depleted waters resulting from partial consumption of dSi in the surface Southern Ocean (Brzezinski & Jones, 2015; de Souza et al., 2015).

6.2. Driving Processes

Dissolved silicon uptake by membrane transporters and silicification are both widespread in eukaryotes and bacteria (Marron et al., 2016), although bSi production in marine waters is dominated by diatoms. Silicifiers preferentially take up the lighter isotopes of silicon during biomineralization. As such, significant depletion or utilization of dSi by diatoms in surface waters results in progressive distillation of dSi, imparting an isotopic enrichment to the remaining dSi and the characteristic depth profile shown in Figure 4d (see also Figure 1). This distillation can be modeled as a Rayleigh-type closed process or a steady-state open system (Equations 5 and 6, respectively), assuming a known starting $\delta^{30}\text{Si}$ of dSi value and a constant biological isotopic fractionation (De La Rocha et al., 1997; Varela et al., 2004). These equations rely on a number of

challenging assumptions regarding the nature of fractionation by different silicifiers, a unique, well-characterized dSi source, and the environmental controls on isotopic uptake during growth (Sutton et al., 2018).

6.3. Sedimentary Archives for $\delta^{30}\text{Si}$

The use of Si stable isotopes as a paleoceanographic proxy was established in the late 1990s based on its similarities to C and N isotope systems (De La Rocha et al., 1997, 1998). Initially, the influence of potentially confounding factors to this proxy, such as a variable isotopic fractionation (i.e., due to temperature), other planktic consumers of dSi (e.g., radiolaria and silicoflagellates), and the influence of dissolution on Si isotopic fractionation, were found to have a negligible effect or were not considered. Since the late 1990s, experimental studies have highlighted potential biases concerning the usefulness of this proxy (Demarest et al., 2009; Sutton et al., 2013) that continue to be debated. The seasonal evolution of biogenic opal $\delta^{30}\text{Si}$ exported into deep sediment traps (Closset et al., 2015; Varela et al., 2004), the good agreement found between core tops and their mixed layer diatom counterparts (Egan et al., 2012), and the lack of a noticeable isotopic change during dissolution either in sediments (Wetzel et al., 2014) or in deep settling diatoms (Fripiat et al., 2012) confirm the rationale behind the use of the proxy. Similar to C and N isotopes, a change in the quantity of Si supplied and/or the source isotopic composition can influence the $\delta^{30}\text{Si}$ of diatoms in the sediment archives (recently highlighted by the very low $\delta^{30}\text{Si}$ of $<0\text{‰}$ for *Ethmodiscus rex*, Xiong et al., 2015), and should be considered when interpreting their geochemistry for paleoceanographic reconstructions. The $\delta^{30}\text{Si}$ of siliceous marine sponges is strikingly correlated to dSi concentration (Hendry et al. 2010; Wille et al., 2010) and provides a paleo-proxy of the dSi supply to the mixed layer, which can be used to better constrain, for example, net dSi uptake by diatoms. Thus, the $\delta^{30}\text{Si}$ of different silicifiers preserved in marine sediment cores, especially when combined with other sedimentary and geochemical archives (e.g., Ge/Si ratio, Shemesh et al., 1988), provides additional constraints on past changes of the silicon cycle over geological timescales.

6.4. Sources of Uncertainty

In addition to the previously discussed process-related biases, the use of $\delta^{30}\text{Si}$ as an ad hoc proxy for the marine Si cycle and/or diatom contribution to paleo-productivity and export and its interpretation can also be influenced by differences in methodology and currently poorly constrained sources of error (e.g., diagenesis; Sutton et al., 2018). An important challenge for $\delta^{30}\text{Si}$ measurements and their interpretation in the paleo-records is ensuring that the biogenic opal is free of contaminating sources of Si (e.g., clay, authigenic Al-Si; Ehlert et al., 2016). Therefore, it is strongly suggested that all protocols used to clean bSi for $\delta^{30}\text{Si}$ measurement ensure frequent visual inspection of the samples (Sutton et al., 2018).

The relationship between dSi isotopic composition and its utilization is relatively straightforward if assuming a single and constant dSi source from below and a constant isotopic enrichment factor (see Equations 5 and 6). However, it should be kept in mind that $\delta^{30}\text{Si}$ may reflect the productivity of silicifiers but not total productivity, as these two processes can be decoupled, resulting in a number of challenges. First, Si is only considered to be a nutrient for silicifiers, that is, not for the entire autotrophic community. Second, diatoms are not the sole autotrophic silicifier. Several recent studies have reported a significant contribution of picoplankton to the bSi stock (Baines et al., 2012; Krause et al. 2017). Their estimated contribution at a global ocean scale is relatively small ($<10\%$ according to the recent review of Tréguer et al., 2021) but will vary regionally. This represents an uncertainty for the use of Si isotope in (paleo-)oceanography since the Si isotopic fractionation of these organisms is unknown. Third, the Si demand, relative to C and N, can vary. For instance, shipboard incubations have shown that Si:N uptake by diatoms can increase by a factor of 3 when the substrate is Fe-limited (Brzezinski et al., 2002; Hutchins & Bruland, 1998) as compared to the typical “Brzezinski” Si:N ratio of 1 for Fe-rich culture experiments (Brzezinski, 1985).

Further, processes using Si (e.g., silicification) and C and N (e.g., photosynthesis) are decoupled when diatoms are evaluated under light-, N- or P-limited conditions (Claquin et al., 2002). However, these results cannot necessarily be applied to natural marine environments. For example, Lasbleiz et al. (2014) reported that heavily silicified diatoms species have higher Si:N ratios above the Kerguelen Plateau, which is

naturally fertilized by Fe, when compared to the surrounding HNLC region of the Southern Ocean. This supposition was confirmed by higher Si:N phytoplankton uptake measured by Closset et al. (2014). The aforementioned results go against a higher Si:N uptake when diatoms are Fe-limited. It therefore seems that the response of Si demand to Fe replete or deplete conditions cannot be generalized simply from Fe addition experiments and needs further study.

7. Applications

C, N, and Si isotopes in marine sediments have been vital for reconstructing changing ocean C and nutrient cycling over a range of timescales. Here, we provide examples of such applications, focusing on Late Quaternary glacial-interglacial cycles and longer-term changes throughout the Cenozoic.

7.1. Late Quaternary Glacial-Interglacial Cycles

The discovery of glacial-interglacial cycles in atmospheric $p\text{CO}_2$ (Figure 5a) has motivated over 40 years of studies into their origin. Early on, it was recognized that ocean chemistry must be related to these $p\text{CO}_2$ variations (Broecker, 1982). Here, we discuss selected $\delta^{13}\text{C}$, $\delta^{15}\text{N}$, and $\delta^{30}\text{Si}$ records that speak to changing nutrient utilization and deep ocean carbon properties since 50,000 years ago (50 ka). Many suitable reconstructions exist for this time interval; for the sake of brevity, only a few example records are presented. Readers are encouraged to consult the references and recent reviews (Galbraith & Skinner, 2020; Hain et al., 2014; Hendry & Brzezinski, 2014; Sigman et al., 2021; Sutton et al., 2018; Tesdal et al. 2013) for further discussion.

Atmospheric $p\text{CO}_2$ as reconstructed from a composite of Antarctic ice cores declines slightly from 50 to 20 ka with notable short-term $p\text{CO}_2$ maxima at Antarctic Isotope Maxima (AIM) 12 (47 ka) and 8 (38 ka) (Figure 5a) (Bauska et al., 2021; Bereiter et al., 2012). Following the Last Glacial Maximum (LGM) $p\text{CO}_2$ minimum, $p\text{CO}_2$ shows a rapid, three-step increase during deglaciation from 18.1 ka to 11.1 ka (Marcott et al., 2014). The selected sedimentary $\delta^{13}\text{C}$, $\delta^{15}\text{N}$, and $\delta^{30}\text{Si}$ records capture many of these $p\text{CO}_2$ features (Figures 5b–5d), suggesting a tight connection to $p\text{CO}_2$. Below, we examine how these sediment proxy records inform our understanding of the ocean's role in modulating glacial-interglacial atmospheric $p\text{CO}_2$ within the context of Southern Ocean nutrient utilization and the Silicic Acid Leakage Hypothesis.

7.1.1. Southern Ocean Nutrient Utilization

As discussed in Box 1, atmospheric $p\text{CO}_2$ is modulated by the efficiency of the ocean's biological pump. Thus, changes in the efficiency of the biological pump are widely considered to explain at least some fraction of the $p\text{CO}_2$ variations over glacial-interglacial cycles (Galbraith & Skinner, 2020; Hain et al., 2010, 2014; Sigman & Boyle, 2000; Sigman et al., 2010). Recall that the efficiency of the biological pump is set by the ratio of preformed to regenerated nutrients in the deep ocean, and that this ratio is set by nutrient utilization in surface ocean regions of deepwater formation (Box 1; Ito & Follows, 2005; Marinov et al., 2006). Today, a substantial fraction of the deep ocean is ventilated through the Southern Ocean surface, where major nutrient concentrations are high year-round. Therefore, reconstructing past changes in nutrient utilization within Southern Ocean surface waters helps constrain the past efficiency of the biological pump. Here, we explore insights on Southern Ocean nutrient utilization provided by sedimentary $\delta^{13}\text{C}$ and $\delta^{15}\text{N}$ proxies.

Nitrogen isotopes of organic matter bound in planktic foraminifera (FB- $\delta^{15}\text{N}$) and diatoms (DB- $\delta^{15}\text{N}$) record past surface ocean nitrate utilization in the SAZ and AZ, respectively (Figure 5c). Before the LGM, millennial-scale SAZ FB- $\delta^{15}\text{N}$ variations tracked $p\text{CO}_2$ (Figure 5a), iron flux (Figure 5d), and indicators of export production, with higher FB- $\delta^{15}\text{N}$ occurring alongside higher iron flux, higher SAZ export production, and lower $p\text{CO}_2$. This sequence supports changing iron fertilization of the SAZ and associated export production as a direct control on $p\text{CO}_2$ (Jaccard et al., 2013; Martínez-García et al., 2014). At the LGM, higher SAZ FB- $\delta^{15}\text{N}$ and AZ DB- $\delta^{15}\text{N}$ occurred without evidence for changes in mean ocean $\delta^{15}\text{N}_{\text{nitrate}}$ (Galbraith et al., 2013) and thus imply more complete utilization of the NO_3^- supply in Southern Ocean surface waters (Ai et al., 2020; Martínez-García et al., 2014; Studer et al., 2015). In isolation, higher SAZ and AZ microfossil-bound $\delta^{15}\text{N}$ at the LGM argue for a more efficient Southern Ocean biological pump. It is worth noting that paleoproductivity proxies indicate higher export production in the SAZ but lower export production in

the AZ compared to the late Holocene (Jaccard et al., 2013; Kohfeld et al., 2005; Thöle et al., 2019). Taken together, these observations suggest a stronger SAZ biological pump (Martínez-García et al., 2014) alongside reduced nutrient supply to the surface AZ (Ai et al., 2020; Studer et al., 2015), likely due to increased “isolation” of the AZ surface ocean at the LGM (Sigman et al., 2021). Both SAZ FB- $\delta^{15}\text{N}$ and AZ DB- $\delta^{15}\text{N}$ declined during the deglaciation, suggesting that SAZ and AZ nitrate utilization weakened coeval with increasing $p\text{CO}_2$. Intriguingly, AZ DB- $\delta^{15}\text{N}$ continued to decline throughout the Holocene, possibly contributing to the Holocene $p\text{CO}_2$ increase through outgassing of deep ocean CO_2 in the AZ (Studer et al., 2018).

Carbon isotope gradients between surface, intermediate, and bottom dwelling foraminifera have been used to reconstruct inferred changes in the redistribution of C in the ocean interior and its relationship to $p\text{CO}_2$ on glacial-interglacial timescales. Ziegler et al. (2013) used the $\delta^{13}\text{C}$ values of intermediate-dwelling and bottom-dwelling foraminifera to reconstruct the $\delta^{13}\text{C}$ gradient between shallow Subantarctic mode water (SAMW) and circumpolar deep water (CDW) in the SAZ of the South Atlantic Ocean (Figure 5b, teal curve). Before the LGM, substantial millennial-scale shifts in the $\delta^{13}\text{C}$ difference ($\Delta\delta^{13}\text{C}_{\text{SAMW-CDW}}$) have similar timing to changes in Antarctic ice core $p\text{CO}_2$ (Figure 5a), iron flux to the SAZ (Figure 5d), and SAZ FB- $\delta^{15}\text{N}$ (Figure 5c; Martínez-García et al., 2014), as evident at AIM 8 and 12. The highest $\Delta\delta^{13}\text{C}_{\text{SAMW-CDW}}$ since 50 ka occurs during the LGM, suggestive of an increased reservoir of isotopically light C in the deep Southern Ocean relative to intermediate waters. While Ziegler et al. (2013) attribute this to increased SAZ nutrient utilization, higher $\Delta\delta^{13}\text{C}_{\text{SAMW-CDW}}$ may also be explained by a circulation-driven reduction in ventilation of the lower cell compared to the upper cell at the LGM (e.g., Burke & Robinson, 2012). Such changes in ocean circulation and utilization would both contribute to increasing the efficiency of the biological pump, as supported by a global model-data analysis of sedimentary $\delta^{13}\text{C}$ and $\delta^{15}\text{N}$ (Schmittner & Somes, 2016). This water mass $\delta^{13}\text{C}$ gradient breaks down during the deglaciation as $\Delta\delta^{13}\text{C}_{\text{SAMW-CDW}}$ decreases from 23 to 12 ka while $p\text{CO}_2$ rises, suggesting that the efficiency of the biological pump declined during deglaciation. Focusing on the deglaciation, Hertzberg et al. (2016) found a reduced $\delta^{13}\text{C}$ gradient between surface and intermediate-depth foraminifera during two periods of deglacial atmospheric $p\text{CO}_2$ rise. These data further support a less efficient biological pump during deglaciation, although whether this was a consequence of changing deep ocean ventilation versus changing surface nutrient utilization is difficult to assess with $\delta^{13}\text{C}$ records (Section 4.4).

The $\delta^{13}\text{C}$ difference between coexisting epifaunal and shallow infaunal benthic foraminifera ($\Delta\delta^{13}\text{C}_{\text{E-I}}$) has also been used to infer changes in bottom water oxygenation and C storage in the deep ocean on glacial-interglacial timescales. This C reservoir is thought to be a major source of carbon to the atmosphere on glacial-interglacial transitions via the Southern Ocean. Studies from the Atlantic (Gottschalk et al., 2016; Hoogakker et al., 2016, 2015) and Indo-Pacific oceans (Gottschalk et al., 2020; Hoogakker et al., 2018; Jacobel et al., 2020; Umling & Thunell, 2018) utilized the $\Delta\delta^{13}\text{C}_{\text{E-I}}$ proxy to propose that the deep waters of these regions were important C storage sites during glacial periods. For instance, Hoogakker et al. (2018) showed lower $\Delta\delta^{13}\text{C}_{\text{E-I}}$ during the LGM in the equatorial Pacific, with a rapid $\Delta\delta^{13}\text{C}_{\text{E-I}}$ increase between 15 and 11 ka (Figure 5b, gray curve). The $\Delta\delta^{13}\text{C}_{\text{E-I}}$ increase implies improving oxygenation of the deep Pacific and loss of respired carbon from the deep Pacific during the latter phase of deglacial $p\text{CO}_2$ rise. However, note that there are outstanding questions with the $\Delta\delta^{13}\text{C}_{\text{E-I}}$ approach in terms of quantifying bottom water oxygenation or C storage (Jacobel et al., 2020) and, as for the water column $\delta^{13}\text{C}$ reconstructions above, separating the effects of local processes (i.e., export production) from the global signature of respiration and circulation on deep ocean $\delta^{13}\text{C}_{\text{DIC}}$.

7.1.2. Silicic Acid Leakage Hypothesis

In Section 7.1.1, the diatom $\delta^{30}\text{Si}$ record from the AZ (Figure 5e) was not discussed. Intriguingly, this record shows nearly the opposite pattern as the $\delta^{13}\text{C}$ and $\delta^{15}\text{N}$ records, with lower $\delta^{30}\text{Si}$ at the LGM indicating less complete AZ dSi utilization, and higher $\delta^{30}\text{Si}$ during the Holocene indicating more complete AZ dSi utilization (Robinson et al., 2014). These seemingly contradictory observations of past dSi and NO_3^- utilization require additional consideration.

Another potential mechanism to account for natural glacial-interglacial variability in $p\text{CO}_2$ is changes in the biological uptake of C by diatoms—relative to uptake by carbonate producing organisms—in the low latitudes (Brzezinski et al., 2002; Matsumoto & Sarmiento, 2008; Matsumoto et al., 2002). In its original

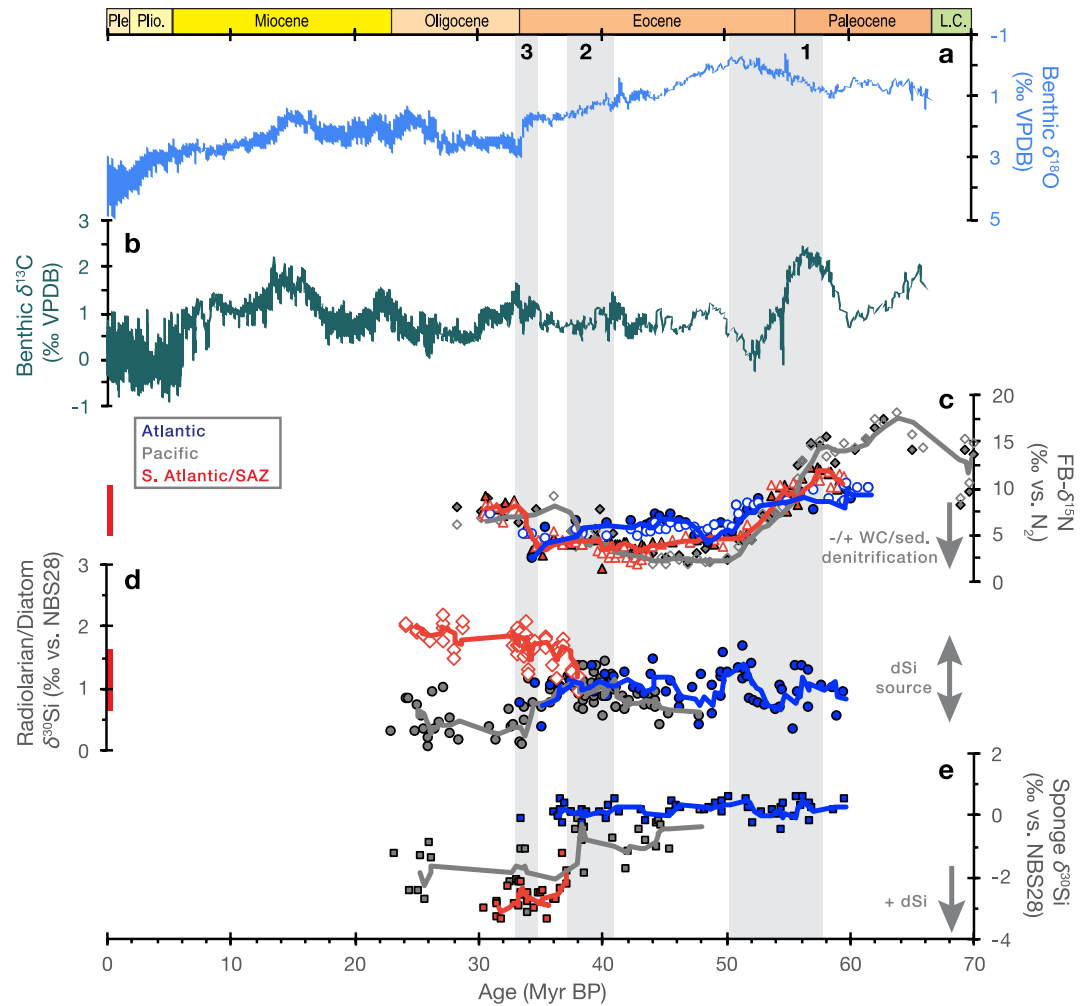


Figure 6. Cenozoic climate and major element isotope variations (all isotope values in ‰ relative to accepted international standards). (a) Global benthic foraminifera $\delta^{18}\text{O}$ and (b) $\delta^{13}\text{C}$ (Zachos et al., 2001). (c) Foraminifera-bound $\delta^{15}\text{N}$ indicating changes in the balance of water column (WC) and sedimentary (sed.) denitrification (Kast et al., 2019). (d) Radiolarian (circles) and diatom (diamonds) $\delta^{30}\text{Si}$ indicating changing dSi sources and (e) sponge $\delta^{30}\text{Si}$ indicating dSi concentration (Egan et al., 2013; Fontorbe et al., 2016, 2017). Blue, gray, and red symbols in (c)–(e) indicate samples from Atlantic, Pacific, and South Atlantic/Subantarctic sediment cores (see individual studies for details). Red vertical lines in (c) and (d) denote the Late Quaternary ranges of Southern Ocean FB- $\delta^{15}\text{N}$ and diatom $\delta^{30}\text{Si}$ in Figure 5. Vertical gray shading denotes three intervals of relevant climatic/tectonic change: (1) closure of the Tethys Sea; (2) formation of the Antarctic Circumpolar Current; (3) Eocene-Oligocene Transition. Time intervals of epochs indicated by colored boxes along top axis (after Walker et al., 2018); “L.C.” is Late Cretaceous, “Plio.” is Pliocene, and “Ple” is Pleistocene.

form, the Silicic Acid Leakage Hypothesis (Brzezinski et al., 2002; Matsumoto et al., 2002) posited that an increased dSi supply to low latitudes relative to other nutrients (specifically NO_3^-) would increase diatom production, lowering $p\text{CO}_2$ by increasing the “rain ratio” of C_{org} to CaCO_3 . The dSi supply to fuel this production has been proposed as originating from dust inputs (Harrison, 2000; Nozaki & Yamamoto, 2001), or “leakage” of intermediate waters with high dSi from the Southern Ocean (Brzezinski et al., 2002; Matsumoto et al., 2002). Later modeling efforts led to the adjustment of the hypothesis to emphasize that it is the “leakage” of high Si:N waters from the Southern Ocean to the low latitudes, rather than an absolute increase in dSi flux and low latitude opal burial, that could drive a reduction in $p\text{CO}_2$ via a shift in the “rain ratio” and oceanic alkalinity (Matsumoto & Sarmiento, 2008).

This hypothesis relies on a mechanism for driving down the Si:N ratio during utilization of major nutrients in the Southern Ocean during glacial periods. This could be due to alleviation of iron limitation as a result

of increased dust-borne iron supply (Figure 5d; Matsumoto et al., 2002), or alternatively due to sea ice expansion or changes in wind dynamics (Matsumoto et al., 2014).

At the LGM, diatom $\delta^{30}\text{Si}$ was lower in the SAZ (Beucher et al., 2007) and AZ (De La Rocha et al., 1998; Robinson et al., 2014) compared to the Holocene (Figure 5e), nearly the opposite pattern from FB- $\delta^{15}\text{N}$ and DB- $\delta^{15}\text{N}$ (Figure 5c). These observations indicate that dSi utilization was lower relative to nitrate in Southern Ocean surface waters during the LGM. Coupling of diatom and sponge silicon isotope records confirms that dSi supply from upwelling outpaced dSi utilization during the LGM and early deglaciation (Figure 5e) (Horn, Beucher, et al., 2011; Robinson et al., 2014). This potentially allowed for the build-up of dSi in the surface Southern Ocean during the LGM, particularly in the Pacific sector (Ellwood et al., 2010), which could then be transported to lower latitudes by northward flowing intermediate water masses.

With regard to the Silicic Acid Leakage Hypothesis, the key test is whether unutilized Southern Ocean dSi was indeed exported to and utilized at low latitudes at the LGM without a concurrent increase in NO_3^- supply. However, low latitude bSi accumulation rate records do not show a clear picture of higher diatom production at the LGM or over the deglaciation (Arellano-Torres et al., 2011; Bradtmiller et al., 2006; Calvo et al., 2011; Dubois et al., 2010; Hayes et al., 2011; S. S. Kienast et al., 2006; Pichevin et al., 2020; Richaud et al., 2007). One record of diatom $\delta^{30}\text{Si}$ and DB- $\delta^{15}\text{N}$ from the eastern equatorial Pacific indicates reduced dSi utilization relative to other nutrients during the LGM, although this most likely reflects changes in local levels of Fe stress (Pichevin et al., 2009). Moreover, sponge spicule $\delta^{30}\text{Si}$ records from low latitudes do not support a significant change in mode water dSi concentrations during the late glacial, except—again—in the case of the Pacific sector (Rousseau et al., 2016). Spicule $\delta^{30}\text{Si}$ records from the LGM onward instead highlight changes in low latitude dSi supply during abrupt climate events in the Atlantic (Hendry et al., 2012, 2016) and Pacific (Doering et al., 2016). These changes in low latitude dSi supply appear as a result of abrupt changes in ocean ventilation (the Silicic Acid Ventilation Hypothesis, Hendry & Brzezinski, 2014) that occur during intervals of increasing $p\text{CO}_2$. In summary, while available data do not support the Silicic Acid Leakage Hypothesis mechanism for lowering glacial $p\text{CO}_2$, Late Quaternary changes in dSi supply and consumption may be an important consideration for the type and amount of biological productivity in different ocean regions.

7.2. Cenozoic

On Cenozoic timescales, marine sediment $\delta^{13}\text{C}$, $\delta^{15}\text{N}$, and $\delta^{30}\text{Si}$ records are challenging to interpret in terms of internal ocean processes such as nutrient utilization (Figure 1, orange box). Instead, changes in external sources and sinks (Figure 1, processes outside orange box) tend to dominate sediment $\delta^{13}\text{C}$, $\delta^{15}\text{N}$, and $\delta^{30}\text{Si}$ on these million-year timescales. Here, we provide an overview of Cenozoic isotopic variability that has been interpreted in the context of external drivers, including large-scale changes in ocean/atmosphere circulation and tectonic events that reshaped ocean gateways.

Stable oxygen isotopes ($\delta^{18}\text{O}$) in benthic foraminifera reveal a gradual cooling of the Earth over the Cenozoic (Figure 6a), superimposed with cyclic variability and sudden warming/cooling events (Zachos et al., 2001, 2008). The long-term Cenozoic $\delta^{13}\text{C}$ record derived from a global compilation of benthic foraminiferal $\delta^{13}\text{C}$ provides insight into the nature of global carbon cycle perturbations (Figure 6b). On the first order, $\delta^{13}\text{C}$ details changes in deep-sea circulation patterns that might trigger or arise from climate changes throughout the Cenozoic (Zachos et al., 2001). Climate warming (e.g., declining $\delta^{18}\text{O}$) during the Paleocene-Eocene Thermal Maximum (PETM, ~56 Ma) was associated with a massive carbon addition to the ocean-atmosphere system that led to a negative $\delta^{13}\text{C}$ excursion in marine carbonates (Zachos et al., 2001). The source of this carbon is debated but has been linked most recently to volcanism associated with the North Atlantic Igneous Province (Gutjahr et al., 2017).

The PETM punctuated a long term, ~2‰ $\delta^{13}\text{C}$ drop between 58 and 52 Ma that may indicate a decrease in organic carbon burial (Komar et al., 2013). During the Early Eocene Climatic Optimum (53–49 Ma), benthic foraminifera $\delta^{13}\text{C}$ increased by ~1‰ without a corresponding shift in benthic $\delta^{18}\text{O}$, possibly indicating a shift in the biological pump and/or ocean circulation under extreme greenhouse conditions (Lauretano et al., 2018). The growth of ice sheets during the Oligocene and Miocene (33.9–5.33 Ma) modulated climate at this time, with $\delta^{13}\text{C}$ and $\delta^{18}\text{O}$ covariance in the early Oligocene and middle Miocene attributed to chang-

ing ocean/atmosphere circulation, ocean productivity, and/or organic carbon burial (Zachos et al., 1997). On ~100 kyr timescales, negative excursions in $\delta^{13}\text{C}$ correspond with negative excursions in $\delta^{18}\text{O}$ for much of the Cenozoic, but this relationship flips after 5 Ma, with negative $\delta^{13}\text{C}$ excursions corresponding with positive $\delta^{18}\text{O}$ excursions for the Plio-Pleistocene. This switch may indicate a fundamental change in the relationship between climate and the carbon cycle during Plio-Pleistocene glaciations (Turner, 2014).

FB- $\delta^{15}\text{N}$ indicates several intervals of profound alteration to the marine nitrogen cycle during the Cenozoic (Kast et al., 2019). Elevated Paleocene FB- $\delta^{15}\text{N}$ (Figure 6c) suggests higher global mean ocean nitrate $\delta^{15}\text{N}$, reflecting an increased rate of global water column denitrification. This is possibly a result of greater production of low-oxygen intermediate-depth waters from more extensive suboxia in the Paleocene ocean due to more widespread shallow seas (Kast et al., 2019). FB- $\delta^{15}\text{N}$ declined from 57 to 50 Ma in the early Eocene, coincident with the early stages of the Asia-India collision and the closure of the Tethys Sea. Low FB- $\delta^{15}\text{N}$ during the middle Eocene suggests that mean ocean nitrate $\delta^{15}\text{N}$ was lower than modern, a possible consequence of higher sedimentary denitrification fluxes caused by a greater area of submerged continental shelves during this period of elevated sea level (Kast et al., 2019). FB- $\delta^{15}\text{N}$ again increased around the Eocene-Oligocene transition at 35 Ma, implying a reduction in sedimentary denitrification associated with the growth of the Antarctic ice sheets. The corresponding sea-level fall would have exposed continental shelves and led to the loss of shelf-hosted sedimentary denitrification (Kast et al., 2019). Future records of nitrogen isotopes may provide higher resolution insights on the marine nitrogen cycle and productivity across key intervals of Earth's Cenozoic climate evolution.

The Cenozoic cooling trend coincided with a rapid diversification and expansion of diatoms, especially at the Eocene-Oligocene boundary and during the mid-Miocene, which may have led to a change in organic carbon burial and a drawdown of atmospheric $p\text{CO}_2$ (Cermeño et al., 2015; Finkel et al., 2005). Concentrations of dSi from the Paleocene onwards have been reconstructed using sponge spicule, radiolarian, and diatom silicon isotopes from marine sediment cores (Figures 6d and 6e). These proxy records suggest that from 60 to 30 Ma, dSi concentrations in the North Atlantic were uniformly low as indicated by elevated sponge spicule $\delta^{30}\text{Si}$ (Figure 6e). These low dSi concentrations may have occurred because Si export by diatoms (and other silicifiers) in excess of new Si supply lowered global dSi before or during the early Cenozoic (Conley et al., 2017; Fontorbe et al., 2016). In the late Eocene, these records suggest that Pacific deep waters experienced an increase in dSi availability at ~37 Ma as indicated by a decline in sponge spicule $\delta^{30}\text{Si}$ (Figure 6e). Increased Pacific dSi availability at this time may have resulted from a shift of deep ocean circulation to Southern Ocean sources with high dSi (Fontorbe et al., 2017). Also at this time, Southern Ocean sponge $\delta^{30}\text{Si}$ declined while diatom $\delta^{30}\text{Si}$ increased (Egan et al., 2013). These shifts are interpreted to represent high deep water dSi and increased dSi utilization in the surface of Southern Ocean coeval with the establishment of a proto-Antarctic Circumpolar Current and high-latitude upwelling at the Eocene-Oligocene boundary (Figure 6d) (Egan et al., 2013).

8. Conclusions

C, N, and Si isotope ratios of marine sediments serve as principal geochemical tools for evaluating past surface ocean nutrient utilization and global C and nutrient cycling. The increasing spatiotemporal coverage of marine sediment isotope datasets and the evolution of new sediment archives (e.g., sponge spicule $\delta^{30}\text{Si}$ and fossil-bound $\delta^{15}\text{N}$) provide compelling evidence for the covariation of Southern Ocean nutrient utilization, the efficiency of the biological pump, nutrient transport, and atmospheric $p\text{CO}_2$ over late Quaternary glacial cycles. On longer timescales, emergent applications of N and Si isotopes in marine sediments are providing new insights into long-term changes in ocean nutrient availability. Alongside existing applications of C isotopes in benthic foraminifera, these reconstructions motivate new research on the connections between global nutrient and C cycles over the Cenozoic.

This review highlights two opportunities for future research. First, multiproxy applications are highly desirable given different impacts from processes at ocean interfaces and internal ocean cycling on each isotope system (Figure 1). Multiproxy applications benefit by both minimizing the potential bias of these non-productivity processes, and providing novel insights gained by concurrent inferences on the uptake of C and major nutrients. Promising examples include the co-application of diatom-bound N and diatom Si isotopes

to Southern Ocean sediments to track variations between past NO_3^- and dSi limitation, and complementary insights on Subantarctic nutrient utilization from water column C isotope gradients and foraminifera-bound N isotopes. Second, the expansion of C, N, and Si isotope proxies to the Cenozoic should greatly improve understanding of long-term C, N, and Si cycles. High-resolution applications of these tools to past Cenozoic climate events could improve knowledge of how ocean C and nutrient cycles facilitated and/or were impacted by these climate changes. Moreover, understanding patterns of ocean C and nutrient cycling and nutrient utilization in past warm climates may be of critical importance for a currently warming world that is on track to surpass any Quaternary climate analog.

Appendix A: GEOTRACES-PAGES Biological Productivity Working Group Members

C. Bolton (CEREGE, Univ. Aix-Marseille, CNRS, IRD, Collège de France, INRAE, Aix-en-Provence, France); E. Calvo (Institut de Ciències del Mar, CSIC, Barcelona, Spain); T. de Gadiel-Thoron (CEREGE, Univ. Aix-Marseille, CNRS, IRD, Collège de France, INRAE Aix-en-Provence, France); S. J. G. Galer (Max Planck Institute for Chemistry, Mainz, Germany); T. J. Horner (NIRVANA Labs & Department of Marine Chemistry & Geochemistry, Woods Hole Oceanographic Institution, Woods Hole, MA USA); F. Lacan (LEGOS, University of Toulouse, CNRS, CNES, IRD, UPS, Toulouse, France); S. H. Little (Department of Earth Sciences, University College London, London, UK); A. J. Lough (National Oceanography Centre, University of Southampton, Southampton, UK; now at School of Geography, University of Leeds, Leeds, UK); A. Tessin (Department of Geology, Kent State University, Kent, OH USA); A. Torfstein (Institute of Earth Sciences, Hebrew University, Jerusalem, & InterUniversity Institute for Marine Sciences, Eilat, Israel); G. Winckler (Lamont-Doherty Earth Observatory of Columbia University, Palisades, NY, USA); K. Wuttig (Antarctic Climate and Ecosystems Cooperative Research Centre, University of Tasmania, Hobart, Australia)

Data Availability Statement

Data sets presented in this research are available via the following repositories and study (listed by Figure): Figures 3 and 4: (1) $\delta^{13}\text{C}_{\text{DIC}}$: (a) CLIVAR P16S (Feely et al., 2008) from GLODAPv2.2020 database (Olsen et al., 2020): <https://www.glodap.info/index.php/merged-and-adjusted-data-product/>. (b) GEOTRACES GA03 (Quay & Wu, 2015) and GP16 (P. Quay, unpublished data) from GEOTRACES IDP2017 (Schlitzer et al., 2018): <https://www.bodc.ac.uk/geotraces/data/idp2017/>. (2) $\delta^{15}\text{N}_{\text{nitrate}}$: (a) CLIVAR P16S (Rafter et al., 2013) from BCO-DMO: <https://www.bco-dmo.org/dataset/651722>. (b) GEOTRACES GA03 (Marconi et al., 2015) and GP16 (Peters et al., 2018) from GEOTRACES IDP2017 (Schlitzer et al., 2018): <https://www.bodc.ac.uk/geotraces/data/idp2017/>. (3) $\delta^{30}\text{Si}$: GEOTRACES GA03 (Brzezinski & Jones, 2015) and GIPY04 (Fripiat et al., 2012) from GEOTRACES IDP2017 (Schlitzer et al., 2018): <https://www.bodc.ac.uk/geotraces/data/idp2017/>. (4) Figure 4a POC Flux (DeVries & Weber, 2017): SIMPLE-TRIM Output from <https://tdevries.eri.ucsb.edu/models-and-data-products/>. Figure 5: (a) Antarctic CO_2 composite: <https://www.ncdc.noaa.gov/paleo-search/study/17975>. (b) $\Delta\delta^{13}\text{C}_{\text{thermocline-deep}}$ from Ziegler et al. (2013) supporting information: <https://www.nature.com/articles/ngeo1782>; $\Delta\delta^{13}\text{C}_{\text{epifaunal-infaunal}}$ (Hoogakker et al., 2018): <https://doi.pangaea.de/10.1594/PANGAEA.891185>. (c) SAZ FB- $\delta^{15}\text{N}$ (Martínez-García et al., 2014): <https://www.ncdc.noaa.gov/paleo/study/18318>; AZ DB- $\delta^{15}\text{N}$ (Studer et al., 2015): <https://doi.pangaea.de/10.1594/PANGAEA.848271>. (d) SAZ Fe flux (Martínez-García et al., 2014): <https://www.ncdc.noaa.gov/paleo/study/18318>. (e) AZ diatom $\delta^{30}\text{Si}$ (Robinson et al., 2014): <https://www.ncdc.noaa.gov/paleo/study/17917>. Figure 6: (a) and (b) Benthic foraminifera $\delta^{18}\text{O}$ and $\delta^{13}\text{C}$ (Zachos et al., 2001): <https://www.ncdc.noaa.gov/paleo/study/8674>. (c) FB- $\delta^{15}\text{N}$ from Kast et al. (2019) supporting information data: <https://science.sciencemag.org/content/suppl/2019/04/24/364.6438.386.DC1>. (d) and (e) Diatom, sponge, and radiolarian $\delta^{30}\text{Si}$ in Egan et al. (2013) supporting information: <https://www.sciencedirect.com/science/article/pii/S0012821X13002185>, Fontorbe et al. (2016) supporting information: <https://www.sciencedirect.com/science/article/pii/S0012821X16304265>, and Fontorbe et al. (2017) supporting information: <https://agupubs.onlinelibrary.wiley.com/doi/full/10.1002/2017PA003090>.

Acknowledgments

The authors thank the organizers, B. Anderson, C. Jeandel, K. Tachikawa, and L. Vidal, and participants of the 2018 GEOTRACES-PAGES joint workshop on trace element and isotope proxies in paleoceanography, from which this manuscript developed. This workshop was funded by the United States National Science Foundation (NSF) through the GEOTRACES program, the international Past Global Changes (PAGES) project, which in turn received support from the Swiss Academy of Sciences and NSF, and the French national program LEFE (Les Enveloppes Fluides et l'Environnement). The authors thank Tim Conway for helpful feedback on a draft manuscript. Mathis Hain and two anonymous reviewers are thanked for insightful comments that greatly improved the manuscript. We thank Noah Planavsky for editorial support, handling, and helpful comments on this manuscript. This study was supported by PAGES, LEFE, and GEOTRACES through NSF. J. R. Farmer acknowledges support from the Max Planck Society, the Tuttle Fund of the Department of Geosciences of Princeton University, the Grand Challenges Program of the Princeton Environmental Institute, and through Exxon Mobil via the Andlinger Center for Energy and the Environment of Princeton University. Open access funding enabled and organized by Projekt DEAL.

References

- Abelson, P. H., & Hoering, T. C. (1961). Carbon isotope fractionation in formation of amino acids by photosynthetic organisms. *Proceedings of the National Academy of Sciences of the United States of America*, *47*(5), 623.
- Ahn, J., & Brook, E. J. (2014). Siple Dome ice reveals two modes of millennial CO₂ change during the last ice age. *Nature Communications*, *5*, 3723. <https://doi.org/10.1038/ncomms4723>
- Ai, X. E., Studer, A. S., Sigman, D. M., Martínez-García, A., Fripiat, F., Thöle, L. M., et al. (2020). Southern ocean upwelling, Earth's obliquity, and glacial-interglacial atmospheric CO₂ change. *Science*, *370*, 1348–1352. <https://doi.org/10.1126/science.abd2115>
- Altabet, M. A., & Francois, R. (1994). Sedimentary nitrogen isotopic ratio as a recorder for surface ocean nitrate utilization. *Global Biogeochemical Cycles*, *8*(1), 103–116.
- Anderson, R. F. (2020). GEOTRACES: Accelerating research on the marine biogeochemical cycles of trace elements and their isotopes. *Annual Review of Marine Science*, *12*, 49–85. <https://doi.org/10.1146/annurev-marine-010318-095123>
- Arellano-Torres, E., Pichevin, L. E., & Ganeshram, R. S. (2011). High-resolution opal records from the eastern tropical Pacific provide evidence for silicic acid leakage from HNLC regions during glacial periods. *Quaternary Science Reviews*, *30*, 1112–1121.
- Baines, S. B., Twining, B. S., Brzezinski, M. A., Krause, J. W., Vogt, S., Assael, D., & McDaniel, H. (2012). Significant silicon accumulation by marine picocyanobacteria. *Nature Geoscience*, *5*(12), 886–891. <https://doi.org/10.1038/ngeo1641>
- Bauska, T., Joos, F., Mix, A., Roth, R., Ahn, J., & Brook, E. J. (2015). Links between atmospheric carbon dioxide, the land carbon reservoir and climate over the past millennium. *Nature Geoscience*, *8*, 383–387.
- Bauska, T., Marcott, S. A., & Brook, E. J. (2021). Abrupt changes in the global carbon cycle during the last glacial period. *Nature Geoscience*, *14*, 91–96. <https://doi.org/10.1038/s41561-020-00680-2>
- Bender, M., Grande, K., Johnson, K., Marra, J., Williams, P. J. L., Sieburth, J., et al. (1987). A comparison of four methods for determining planktonic community production. *Limnology & Oceanography*, *32*(5), 1085–1098.
- Bereiter, B., Lüthi, D., Siegrist, M., Schüpbach, S., Stocker, T. F., & Fischer, H. (2012). Mode change of millennial CO₂ variability during the last glacial cycle associated with a bipolar marine carbon seesaw. *Proceedings of the National Academy of Sciences of the United States of America*, *109*, 9755–9760.
- Berger, W. H., Smetacek, V., & Wefer, G. (1989). Ocean productivity and paleoproductivity—An overview. In W. H. Berger, V. S. Smetacek, G. Wefer (Eds.), (Eds) Productivity of the oceans present and past: Report of the Dahlem workshop on productivity of the ocean, Berlin, 1988, Life Sciences Research Reports (Vol. 44, pp. 1–34). Wiley & Sons.
- Beucher, C. P., Brzezinski, M. A., & Crosta, X. (2007). Silicic acid dynamics in the glacial sub-Antarctic: Implications for the silicic acid leakage hypothesis. *Global Biogeochemical Cycles*, *21*, GB3015. <https://doi.org/10.1029/2006GB002746>
- Bratton, L. L., Anderson, R. F., Fleisher, M. Q., & Burckle, L. H. (2006). Diatom productivity in the equatorial Pacific Ocean from the last glacial period to the present: A test of the silicic acid leakage hypothesis. *Paleoceanography*, *21*, PA4201. <https://doi.org/10.1029/2006PA001282>
- Brandes, J. A., & Devol, A. H. (2002). A global marine fixed nitrogen isotopic budget: Implications for Holocene nitrogen cycling. *Global Biogeochemical Cycles*, *16*, 1120. <https://doi.org/10.1029/2001GB001856>
- Broecker, W. S. (1982). Glacial to interglacial changes in ocean chemistry. *Progress in Oceanography*, *11*, 151–197.
- Broecker, W. S., & Maier-Reimer, E. (1992). The influence of air and sea exchange on the carbon isotope distribution in the sea. *Global Biogeochemical Cycles*, *6*, 315–320.
- Broecker, W. S., & Peng, T. H. (1982). *Tracers in the sea*. Lamont-Doherty Geological Observatory of Columbia University.
- Brzezinski, M. A. (1985). The Si:C ratio of marine diatoms: Interspecific variability and the effect of some environmental variables. *Journal of Phycology*, *21*(3), 347–357.
- Brzezinski, M. A., & Jones, J. L. (2015). Coupling of the distribution of silicon isotopes to the meridional overturning circulation of the North Atlantic Ocean. *Deep Sea Research Part II*, *116*, 79–88. <https://doi.org/10.1016/j.dsr2.2014.11.015>
- Brzezinski, M. A., Sigman, D. M., Sarmiento, J. L., Matsumoto, K., Gruber, N., Rau, G. H., & Coale, K. H. (2002). A switch from Si(OH)₄ to NO₃⁻ depletion in the glacial Southern Ocean. *Geophysical Research Letters*, *29*, 1564. <https://doi.org/10.1029/2001GL014349>
- Burke, A., & Robinson, L. F. (2012). The Southern Ocean's role in carbon exchange during the last deglaciation. *Science*, *335*, 557–561. <https://doi.org/10.1126/science.1208163>
- Calvo, E., Pelejero, C., Pena, L. D., Cacho, I., & Logan, G. A. (2011). Eastern Equatorial Pacific productivity and related-CO₂ changes since the last glacial maximum. *Proceedings of the National Academy of Sciences of the United States of America*, *108*, 5537–5541. <https://doi.org/10.1073/pnas.1009761108>
- Cardinal, D., Alleman, L. Y., Dehairs, F., Savoye, N., Trull, T. W., & André, L. (2005). Relevance of silicon isotopes to Si-nutrient utilization and Si-source assessment in Antarctic waters. *Global Biogeochemical Cycles*, *19*(2), GB2007. <https://doi.org/10.1029/2004GB002364>
- Carpenter, E. J., Harvey, H. R., Fry, B., & Capone, D. G. (1997). Biogeochemical tracers of the marine cyanobacterium *Trichodesmium*. *Deep Sea Research Part I*, *44*, 27–38.
- Casciotti, K. L., Trull, T. W., Glover, D. M., & Davies, D. (2008). Constraints on nitrogen cycling at the subtropical North Pacific Station ALOHA from isotopic measurements of nitrate and particulate nitrogen. *Deep Sea Research Part II*, *55*, 1661–1672.
- Cermeño, P., Falkowski, P. G., Romero, O. E., Schaller, M. F., & Vallina, S. M. (2015). Continental erosion and the Cenozoic rise of marine diatoms. *Proceedings of the National Academy of Sciences of the United States of America*, *112*(14), 4239–4244.
- Claquin, P., Martin-Jezequel, V., Kromkamp, J. C., Veldhuis, M. J. W., & Kraay, G. W. (2002). Uncoupling of silicon compared with carbon and nitrogen metabolisms and the role of the cell cycle in continuous cultures of *Thalassiosira pseudonana* (Bacillariophyceae) under light, nitrogen and phosphorus control. *Journal of Phycology*, *38*(5), 922–930. <https://doi.org/10.1046/j.1529-8817.2002.t01-1-01220.x>
- Cline, J. D., & Kaplan, I. R. (1975). Isotopic fractionation of dissolved nitrate during denitrification in the eastern tropical North Pacific Ocean. *Marine Chemistry*, *3*, 271–299.
- Closset, I., Cardinal, D., Bray, S. G., Thil, F., Djouarav, I., Rigual-Hernández, A. S., & Trull, T. W. (2015). Seasonal variations, origin, and fate of settling diatoms in the Southern Ocean tracked by silicon isotope records in deep sediment traps. *Global Biogeochemical Cycles*, *29*(9), 1495–1510. <https://doi.org/10.1002/2015GB005180>
- Closset, I., Lasbleiz, M., Leblanc, K., Quéguiner, B., Cavagna, A.-J., Elskens, M., et al. (2014). Seasonal evolution of net and regenerated silica production around a natural Fe-fertilized area in the Southern Ocean estimated with Si isotopic approaches. *Biogeosciences*, *11*(20), 5827–5846.
- Conley, D. J., Frings, P. J., Fontorbe, G., Clymans, W., Stadmark, J., Hendry, K. R., et al. (2017). Biosilicification drives a decline of dissolved Si in the oceans through geologic time. *Frontiers in Marine Science*, *4*, 397. <https://doi.org/10.3389/fmars.2017.00397>

- Coplen, T. B. (2011). Guidelines and recommended terms for expression of stable-isotope-ratio and gas-ratio measurement results. *Rapid Communications in Mass Spectrometry*, 25, 2538–2560. <https://doi.org/10.1002/rcm.5129>
- Coplen, T. B., Böhlke, J. K., De Bièvre, P., Ding, T., Holden, N. E., Hopple, J. A., et al. (2002). Isotope-abundance variations of selected elements. *Pure and Applied Chemistry*, 74, 1987–2017.
- Coplen, T. B., Brand, W. A., Gehre, M., Gröning, M., Meijer, H. A. J., Toman, B., & Verkouteren, R. M. (2006). New Guidelines for d13C measurements. *Analytical Chemistry*, 78, 2439–2441. <https://doi.org/10.1021/ac052027c>
- Costa, K. M., Hayes, C. M., Anderson, R. F., Pavia, F. J., Bausch, A., Deng, F., et al. (2020). ²³⁰Th normalization: New insights on an essential tool for quantifying sedimentary fluxes in the modern and Quaternary ocean. *Paleoceanography and Paleoclimatology*, 35. <https://doi.org/10.1029/2019PA003820>
- Curry, W. B., & Oppo, D. W. (2005). Glacial water mass geometry and the distribution of δ¹³C of ΣCO₂ in the western Atlantic Ocean. *Paleoceanography*, 20, PA1017.
- Degens, E. T., Guillard, R. R. L., Sackett, W. M., & Hellebust, J. A. (1968). Metabolic fractionation of carbon isotopes in marine plankton—I. Temperature and respiration experiments. *Deep-Sea Research*, 15(1), 1–9.
- De La Rocha, C. L., Brzezinski, M. A., & DeNiro, M. J. (1997). Fractionation of silicon isotopes by marine diatoms during biogenic silica formation. *Geochimica et Cosmochimica Acta*, 61(23), 5051–5056.
- De La Rocha, C. L., Brzezinski, M. A., DeNiro, M. J., & Shemesh, A. (1998). Silicon isotope composition of diatoms as an indicator of past oceanic change. *Nature*, 395, 680–683.
- Demarest, M. S., Brzezinski, M. A., & Beucher, C. P. (2009). Fractionation of silicon isotopes during biogenic silica dissolution. *Geochimica et Cosmochimica Acta*, 73(19), 5572–5583. <https://doi.org/10.1016/j.gca.2009.06.019>
- de Souza, G. F., Slater, R. D., Hain, M. P., Brzezinski, M. A., & Sarimento, J. L. (2015). Distal and proximal controls on the silicon stable isotope signature of North Atlantic Deep Water. *Earth and Planetary Science Letters*, 432, 342–353. <https://doi.org/10.1016/j.epsl.2015.10.025>
- Deutsch, C., Sigman, D. M., Thunell, R. C., Meckler, A. N., & Haug, G. H. (2004). Isotopic constraints on glacial/interglacial changes in the oceanic nitrogen budget. *Global Biogeochemical Cycles*, 18, GB4012. <https://doi.org/10.1029/2003GB002189>
- DeVries, T., & Weber, T. (2017). The export and fate of organic matter in the ocean: New constraints from combining satellite and oceanographic tracer observations. *Global Biogeochemical Cycles*, 31, 535–555. <https://doi.org/10.1002/2016GB005551>
- Doering, K., Erdem, Z., Ehler, C., Fleury, S., Frank, M., & Schneider, R. (2016). Changes in diatom productivity and upwelling intensity off Peru since the Last Glacial Maximum: Response to basin-scale atmospheric and oceanic forcing. *Paleoceanography*, 31(10), 1453–1473.
- Dubois, N., Kienast, M., Kienast, S., Calvert, S. E., Francois, R., & Anderson, R. F. (2010). Sedimentary opal records in the eastern equatorial Pacific: It's not all about leakage. *Global Biogeochemical Cycles*, 24, GB4020. <https://doi.org/10.1029/2010GC003821>
- Dugdale, R. C., & Goering, J. J. (1967). Uptake of new and regenerated forms of nitrogen in primary production. *Limnology & Oceanography*, 12(2), 196–206.
- Egan, K. E., Rickaby, R. E. M., Hendry, K. R., & Halliday, A. N. (2013). Opening the gateways for diatoms primes Earth for Antarctic glaciation. *Earth and Planetary Science Letters*, 375, 34–43. <https://doi.org/10.1016/j.epsl.2013.04.030>
- Egan, K. E., Rickaby, R. E. M., Leng, M. J., Hendry, K. R., Hermoso, M., Sloane, H. J., et al. (2012). Diatom silicon isotopes as a proxy for silicic acid utilisation: A Southern Ocean core top calibration. *Geochimica et Cosmochimica Acta*, 96, 174–192. <https://doi.org/10.1016/j.gca.2012.08.002>
- Ehler, C., Doering, K., Wallmann, K., Scholz, F., Sommer, S., Grasse, P., et al. (2016). Stable silicon isotope signatures of marine pore waters—Biogenic opal dissolution versus authigenic clay mineral formation. *Geochimica et Cosmochimica Acta*, 191, 102–117. <https://doi.org/10.1016/j.gca.2016.07.022>
- Eide, M., Olsen, A., Ninnemann, U. S., & Eldevik, T. (2017). A global estimate of the full oceanic ¹³C Suess effect since the preindustrial. *Global Biogeochemical Cycles*, 31, 492–514.
- Ellwood, M. J., Wille, M., & Maher, W. (2010). Glacial silicic acid concentrations in the Southern Ocean. *Science*, 330, 1088–1091.
- Eppley, R. W., & Peterson, B. J. (1979). Particulate organic matter flux and planktonic new production in the deep ocean. *Nature*, 282(5740), 677–680.
- Eugster, O., Gruber, N., Deutsch, C., Jaccard, S. L., & Payne, M. R. (2013). The dynamics of the marine nitrogen cycle across the last deglaciation. *Paleoceanography*, 28, 116–129. <https://doi.org/10.1002/palo.20020>
- Fawcett, S. E., Lomas, M., Casey, J. R., Ward, B. B., & Sigman, D. M. (2011). Assimilation of upwelled nitrate by small eukaryotes in the Sargasso Sea. *Nature Geoscience*, 4(10), 717–722. <https://doi.org/10.1038/ngeo1265>
- Feeley, R. A., Sabine, C. L., Millero, F. J., Langdon, C., Dickson, A. G., Fine, R. A., et al. (2008). Carbon dioxide, hydrographic, and chemical data obtained during the R/Vs Roger Revelle and Thomas G. Thompson repeat hydrography cruises in the Pacific Ocean: CLIVAR CO₂ sections P16S_2005 and P16N_2006. In A. Kozyr (Ed.), *ORNL/CDIAC-155, NDP-090* (p. 54). Carbon Dioxide Information Analysis Center, Oak Ridge National Laboratory, U.S. Department of Energy. <https://doi.org/10.3334/CDIAC/00002>
- Finkel, Z. V., Katz, M. E., Wright, J. D., Schofield, O. M., & Falkowski, P. G. (2005). Climatically driven macroevolutionary patterns in the size of marine diatoms over the Cenozoic. *Proceedings of the National Academy of Sciences of the United States of America*, 102(25), 8927–8932.
- Fogel, M. L., & Cifuentes, L. A. (1993). Isotope fractionation during primary production. In M. H. Engel & S. A. Macko (Eds.), *Organic geochemistry* (pp. 73–98). Plenum Press.
- Fontorbe, G., Frings, P. J., Christina, L., Hendry, K. R., & Conley, D. J. (2016). A silicon depleted North Atlantic since the Palaeogene: Evidence from sponge and radiolarian silicon isotopes. *Earth and Planetary Science Letters*, 453, 67–77.
- Fontorbe, G., Frings, P. J., De La Rocha, C. L., Hendry, K. R., Carstensen, J., & Conley, D. J. (2017). Enrichment of dissolved silica in the deep Equatorial Pacific during the Eocene-Oligocene. *Paleoceanography*, 32(8), 848–863.
- Freudenthal, T., Wagner, T., Wenzhofer, F., Zabel, M., & Wefer, G. (2001). Early diagenesis of organic matter from sediments of the eastern subtropical Atlantic: Evidence from stable nitrogen and carbon isotopes. *Geochimica et Cosmochimica Acta*, 65, 1795–1808.
- Frings, P. J., Clymans, W., Fontorbe, G., De La Rocha, C. L., & Conley, D. J. (2016). The continental Si cycle and its impact on the ocean Si isotope budget. *Chemical Geology*, 425, 12–36. <https://doi.org/10.1016/j.chemgeo.2016.01.020>
- Fripiat, F., Cavagna, A.-J., Dehairs, F., de Brauwere, A., André, L., & Cardinal, D. (2012). Processes controlling the Si-isotopic composition in the Southern Ocean and application for paleoceanography. *Biogeosciences*, 9, 2443–2457.
- Fripiat, F., Martínez-García, A., Fawcett, S. E., Kemeny, P. C., Studer, A. S., Smart, S. M., et al. (2019). The isotope effect of nitrate assimilation in the Antarctic Zone: Improved estimates and paleoceanographic implications. *Geochimica et Cosmochimica Acta*, 247, 261–279. <https://doi.org/10.1016/j.gca.2018.12.003>

- Galbraith, E. D., & Jaccard, S. L. (2015). Deglacial weakening of the oceanic soft tissue pump: Global constraints from sedimentary nitrogen isotopes and oxygenation proxies. *Quaternary Science Reviews*, *109*, 38–48.
- Galbraith, E. D., Kienast, M., Jaccard, S. L., Pedersen, T. F., Brunelle, B. G., Sigman, D. M., & Kiefer, T. (2008). Consistent relationship between global climate and surface nitrate utilization in the western subarctic Pacific throughout the last 500 ka. *Paleoceanography*, *23*(2). <https://doi.org/10.1029/2007pa001518>
- Galbraith, E. D., Kienast, M., & NICOPP Working Group Members (2013). The acceleration of oceanic denitrification during deglacial warming. *Nature Geoscience*, *6*, 579–584.
- Galbraith, E. D., Kwon, E. Y., Bianchi, D., Hain, M. P., & Sarmiento, J. L. (2015). The impact of atmospheric pCO₂ on carbon isotope ratios of the atmosphere and ocean. *Global Biogeochemical Cycles*, *29*, 307–324. <https://doi.org/10.1002/2014GB004929>
- Galbraith, E. D., & Skinner, L. C. (2020). The biological pump during the Last Glacial Maximum. *Annual Review of Marine Science*, *12*, 559–586. <https://doi.org/10.1146/annurev-marine-010419-010906>
- Gaye, B., Nagel, B., Dähnke, K., Rixen, T., & Emeis, K.-C. (2013). Evidence of parallel denitrification and nitrite oxidation in the ODZ of the Arabian Sea from paired stable isotopes of nitrate and nitrite. *Global Biogeochemical Cycles*, *27*, 1059–1071. <https://doi.org/10.1002/2011GB004115>
- Gaye-Haake, B., Lahajnar, N., Emeis, K.-C., Unger, D., Rixen, T., Suthhof, A., et al. (2005). Stable nitrogen isotopic ratios of sinking particles and sediments from the northern Indian Ocean. *Marine Chemistry*, *96*, 243–255. <https://doi.org/10.1016/j.marchem.2005.02.001>
- Gottschalk, J., Michel, E., Thöle, L. M., Studer, A. S., Hasenfratz, A. P., Schmid, N., et al. (2020). Glacial heterogeneity in Southern Ocean carbon storage abated by fast South Indian deglacial carbon release. *Nature Communications*, *11*, 6192. <https://doi.org/10.1038/s41467-020-20034-1>
- Gottschalk, J., Skinner, L. C., Lippold, J., Vogel, H., Frank, N., Jaccard, S. L., & Waelbroeck, C. (2016). Biological and physical controls in the Southern Ocean on past millennial-scale atmospheric CO₂ changes. *Nature Communications*, *7*, 11539. <https://doi.org/10.1038/ncomms11539>
- Gutjahr, M., Ridgwell, A., Sexton, P. F., Anagnostou, E., Pearson, P. N., Pälike, H., et al. (2017). Very large release of mostly volcanic carbon during the Palaeocene-Eocene thermal maximum. *Nature*, *548*, 573–577. <https://doi.org/10.1038/nature23646>
- Hain, M. P., Sigman, D. M., & Haug, G. H. (2010). Carbon dioxide effects of Antarctic stratification, North Atlantic Intermediate Water formation, and subantarctic nutrient drawdown during the last ice age: Diagnosis and synthesis in a geochemical box model. *Global Biogeochemical Cycles*, *24*, GB4023. <https://doi.org/10.1029/2010GB003790>
- Hain, M. P., Sigman, D. M., & Haug, G. H. (2014). The biological pump in the past. In *Treatise on geochemistry* (2nd ed., pp. 485–517). Elsevier.
- Harrison, K. G. (2000). Role of increased marine silica input on paleo-pCO₂ levels. *Paleoceanography*, *15*, 292–298.
- Hayes, C. T., Anderson, R. F., & Fleisher, M. Q. (2011). Opal accumulation rates in the equatorial Pacific and mechanisms of deglaciation. *Paleoceanography*, *26*, PA1207. <https://doi.org/10.1029/2010PA002008>
- Hendry, K. R., & Brzezinski, M. A. (2014). Using silicon isotopes to understand the role of the Southern Ocean in modern and ancient biogeochemistry and climate. *Quaternary Science Reviews*, *89*, 13–26.
- Hendry, K. R., Gong, X., Knorr, G., Pike, J., & Hall, I. R. (2016). Deglacial diatom production in the tropical North Atlantic driven by enhanced silicic acid supply. *Earth and Planetary Science Letters*, *438*, 122–129.
- Hendry, K. R., Leng, M. J., Robinson, L. F., Sloane, H. J., Blusztjan, J., Rickaby, R. E. M., et al. (2010). Silicon isotopes in Antarctic sponges: An interlaboratory comparison. *Antarctic Science*, *23*(1), 34–42. <https://doi.org/10.1017/S0954102010000593>
- Hendry, K. R., Robinson, L. F., Meredith, M. P., Mülitz, S., Chiessi, C. M., & Arz, H. (2012). Abrupt changes in high-latitude nutrient supply to the Atlantic during the last glacial cycle. *Geology*, *40*(2), 123–126.
- Hertzberg, J. E., Lund, D. C., Schmittner, A., & Skrivaneck, L. (2016). Evidence for a biological pump driver of atmospheric CO₂ rise during Heinrich Stadial 1. *Geophysical Research Letters*, *43*, 12242–12251.
- Higgins, M. B., Robinson, R. S., Casciotti, K. L., McIlvin, M. R., & Pearson, A. (2009). A method for determining the nitrogen isotopic composition of porphyrins. *Analytical Chemistry*, *81* (1), 184–192. <https://doi.org/10.1021/ac8017185>
- Hoering, T. C., & Ford, H. T. (1960). The isotope effect in the fixation of nitrogen by *Azotobacter*. *Journal of the American Chemical Society*, *82*, 376–378.
- Hoogakker, B. A., Thornalley, D. J. R., & Barker, S. (2016). Millennial changes in North Atlantic oxygen concentrations. *Biogeosciences*, *13*, 211–221. <https://doi.org/10.5194/bg-13-211-2016>
- Hoogakker, B. A. A., Elderfield, H., Schmiel, G., McCave, I. N., & Rickaby, R. E. M. (2015). Glacial-interglacial changes in bottom-water oxygen content on the Portuguese margin. *Nature Geoscience* *8* (1), 40–43.
- Hoogakker, B. A. A., Lu, Z., Umling, N., Jones, L., Zhou, X., Rickaby, R. E. M., et al. (2018). Glacial expansion of oxygen-depleted seawater in the eastern tropical Pacific. *Nature* *242*, 240.
- Horn, M. G., Beucher, C., Robinson, R. S., & Brzezinski, M. A. (2011). Southern Ocean nitrogen and silicon dynamics during the last deglaciation. *Earth and Planetary Science Letters*, *310*, 334–339.
- Horn, M. G., Robinson, R. S., Rynearson, T. A., & Sigman, D. M. (2011). Nitrogen isotopic relationship between diatom-bound and bulk organic matter of cultured polar diatoms. *Paleoceanography*, *26*, PA3208. <https://doi.org/10.1029/2010PA002080>
- Horner, T. J., Little, S. H., Conway, T. M., Farmer, J. R., Hertzberg, J. H., Lough, A., et al. (2021). Bioactive trace metals and their isotopes as paleoproductivity proxies: An assessment using GEOTRACES-era data. *Global Biogeochemical Cycles*, e2020GB006814. Retrieved from <https://agupubs.onlinelibrary.wiley.com/doi/abs/10.1029/2020GB006814>
- Hutchins, D. A., & Bruland, K. W. (1998). Iron-limited diatom growth and Si:N uptake ratios in a coastal upwelling regime. *Nature*, *393*, 65–68.
- Ito, T., & Follows, M. J. (2005). Preformed phosphate, soft tissue pump and atmospheric CO₂. *Journal of Marine Research*, *63*(4), 813–839.
- Jaccard, S. L., Hayes, C. T., Martínez-García, A., Hodell, D. A., Anderson, R. F., Sigman, D. M., & Haug, G. H. (2013). Two modes of change in Southern Ocean productivity over the past million years. *Science*, *339*, 1419–1423. <https://doi.org/10.1126/science.1227545>
- Jacobel, A. W., Anderson, R. F., Jaccard, S. L., McManus, J. F., Pavia, F. J., & Winckler, G. (2020). Deep Pacific storage of respired carbon during the last ice age: Perspectives from bottom water oxygen reconstructions. *Quaternary Science Reviews*, *230*. <https://doi.org/10.1016/j.quascirev.2019.106065>
- Kast, E. R., Stolper, D. A., Auderset, A., Higgins, J. A., Ren, H., Wang, X. T., et al. (2019). Nitrogen isotope evidence for expanded ocean suboxia in the early Cenozoic. *Science*, *364*, 386–389. <https://doi.org/10.1126/science.aau5784>
- Keeling, C. D. (1979). The Suess effect: ¹³carbon-¹⁴carbon interrelations. *Environment International*, *2*(4–6), 229–300.
- Keeling, R. F., Graven, H. D., Welp, L. R., Resplandy, L., Bi, J., Piper, S. C., et al. (2017). Trend in ¹³C discrimination of land photosynthesis. *Proceedings of the National Academy of Sciences of the United States of America*, 201619240.

- Kemeny, P. C., Kast, E. R., Hain, M. P., Fawcett, S. E., Fripiat, F., Studer, A. S., et al. (2018). A seasonal model of nitrogen isotopes in the ice age Antarctic Zone: Support for weakening of the Southern Ocean upper overturning cell. *Paleoceanography and Paleoclimatology*, 33, 1453–1471.
- Kienast, M., Higginson, M. J., Mollenhauer, G., Eglinton, T. I., Chen, M.-T., & Calvert, S. E. (2005). On the sedimentological origin of down-core variations of bulk sedimentary nitrogen isotope ratios. *Paleoceanography*, 20, PA2009. <https://doi.org/10.1029/2004PA001081>
- Kienast, S. S., Kienast, M., Jaccard, S. L., Calvert, S. E., & Francois, R. (2006). Testing the silica leakage hypothesis with sedimentary opal records from the eastern equatorial Pacific over the last 150 kyrs. *Geophysical Research Letters*, 33, L15607. <https://doi.org/10.1029/12006GL026651>
- Knapp, A. N., Difiore, P. J., Deutsch, C., Sigman, D. M., & Lipschultz, F. (2008). Nitrate isotopic composition between Bermuda and Puerto Rico: Implications for N₂ fixation in the Atlantic Ocean. *Global Biogeochemical Cycles*, 22, GB3014.
- Kohfeld, K. E., LaQu re, C., Harrison, S. P., & Anderson, R. F. (2005). Role of marine biology in glacial-interglacial CO₂ cycles. *Science*, 308, 74–78. <https://doi.org/10.1126/science.1105375>
- Komar, N., Zeebe, R. E., & Dickens, G. R. (2013). Understanding long-term carbon cycle trends: The late Paleocene through the early Eocene. *Paleoceanography*, 28, 650–662. <https://doi.org/10.1002/palo.20060>
- Krause, J. W., Brzezinski, M. A., Baines, S. B., Collier, J. L., Twining, B. S., & Ohnemus, D. C. (2017). Picoplankton contribution to biogenic silica stocks and production rates in the Sargasso Sea. *Global Biogeochemical Cycles*, 31, 762–774. <https://doi.org/10.1002/2017GB005619>
- Kroopnick, P. M. (1974). Correlations between ¹³C and ΣCO₂ in surface waters and atmospheric CO₂. *Earth and Planetary Science Letters*, 22, 397–403.
- Kroopnick, P. M. (1985). The distribution of ¹³C of ΣCO₂ in the world oceans. *Deep Sea Research Part A*, 32, 57–84.
- Lasbleiz, M., Leblanc, K., Blain, S., Ras, J., Cornet-Barthaux, V., H lias Nunige, S., & Qu guiner, B. (2014). Pigments, elemental composition (C, N, P, and Si), and stoichiometry of particulate matter in the naturally iron fertilized region of Kerguelen in the Southern Ocean. *Biogeosciences*, 11, 5931–5955. <https://doi.org/10.5194/bg-11-5931-2014>
- Lauretano, V., Zachos, J. C., & Lourens, L. J. (2018). Orbitally paced carbon and deep-sea temperature changes at the peak of the Early Eocene Climatic Optimum. *Paleoceanography and Paleoclimatology*, 33, 1050–1065.
- Lauvset, S. K., Key, R. M., Olsen, A., van Heuven, S., Velo, A., Lin, X., et al. (2016). A new global interior ocean mapped climatology: The 1° by 1° GLODAP version 2. *Earth System Science Data*, 8, 325–340.
- Lehmann, M. F., Sigman, D. M., McCorkle, D. C., Granger, J., Hoffman, S., Cane, G., & Brunelle, B. G. (2007). The distribution of nitrate ¹⁵N/¹⁴N in marine sediments and the impact of benthic nitrogen loss on the isotopic composition of oceanic nitrate. *Geochimica et Cosmochimica Acta*, 71, 538405494. <https://doi.org/10.1016/j.gca.2007.07.025>
- LeKieffre, C., Spero, H. J., Fehrenbacher, J. S., Russell, A. D., Ren, H., Geslin, E., & Meibom, A. (2020). Ammonium is the preferred source of nitrogen for planktonic foraminifer and their dinoflagellate symbionts. *Proceedings of the Royal Society B: Biological Sciences*, 287. <https://doi.org/10.1098/rspb.2020.0620>
- Lynch-Stieglitz, J., Stocker, T. F., Broecker, W. S., & Fairbanks, R. G. (1995). The influence of air-sea exchange on the isotopic composition of oceanic carbon: Observations and modeling. *Global Biogeochemical Cycles* 9, 653–665.
- MacFarling Meure, C., Etheridge, D., Trudinger, C., Steele, P., Langenfelds, R., van Ommen, T., et al. (2006). Law Dome CO₂, CH₄ and N₂O ice core records extended to 2000 years BP. *Geophysical Research Letters*, 33, L14810. <https://doi.org/10.1029/2006GL026152>
- Marconi, D., Weigand, M. A., Raftar, P. A., McIlbin, M. R., Forbes, M., Casciotti, K. L., & Sigman, D. M. (2015). Nitrate isotope distributions on the US GEOTRACES North Atlantic cross-basin section: Signals of polar nitrate sources and low latitude nitrogen cycling. *Marine Chemistry*, 177, 143–156. <https://doi.org/10.1016/j.marchem.2015.06.007>
- Marcott, S. A., Bauska, T. K., Buizert, C., Steig, E. J., Rosen, J. L., Cuffey, K. M., et al. (2014). Centennial-scale changes in the global carbon cycle during the last deglaciation. *Nature*, 514, 616–619.
- Marinov, I., Gnanadesikan, A., Toggweiler, J. R., & Sarmiento, J. L. (2006). The Southern Ocean biogeochemical divide. *Nature*, 441(7096), 964–967.
- Mariotti, A. (1983). Atmospheric nitrogen is a reliable standard for natural ¹⁵N abundance measurements. *Nature*, 303, 685–687.
- Mariotti, A., Germon, J. C., Hubert, P., Kaiser, P., Letolle, R., Tardieu, A., & Tardieu, P. (1981). Experimental determination of nitrogen kinetic isotope fractionation: Some principles; illustration for the denitrification and nitrification processes. *Plant and Soil*, 62(3), 413–430.
- Marron, A. O., Ratcliffe, S., Wheeler, G. L., Goldstein, R. E., King, N., Not, F., et al. (2016). The evolution of silicon transport in eukaryotes. *Molecular Biology and Evolution*, 33(12), 3226–3248.
- Martinez-Garcia, A., Sigman, D. M., Ren, H., Anderson, R. F., Straub, M., Hodell, D. A., et al. (2014). Iron fertilization of the Subantarctic Ocean during the last ice age. *Science*, 343, 1347–1350. <https://doi.org/10.1126/science.1246848>
- Matsumoto, K. (2007). Biology-mediated temperature control on atmospheric pCO₂ and ocean biogeochemistry. *Geophysical Research Letters*, 34, L20605. <https://doi.org/10.1029/2007GL031301>
- Matsumoto, K., Chase, Z., & Kohfeld, K. (2014). Different mechanisms of silicic acid leakage and their biogeochemical consequences. *Paleoceanography*, 29(3), 238–254.
- Matsumoto, K., & Sarmiento, J. L. (2008). A corollary to the silicic acid leakage hypothesis. *Paleoceanography*, 23, PA2203. <https://doi.org/10.1029/2007PA001515>
- Matsumoto, K., Sarmiento, J. L., & Brzezinski, M. A. (2002). Silicic acid leakage from the Southern Ocean: A possible explanation for glacial atmospheric pCO₂. *Global Biogeochemical Cycles*, 16, 1031. <https://doi.org/10.1029/2001GB001442>
- McCarthy, M. D., Lehman, J., & Kudela, R. (2013). Compound-specific amino acid δ¹⁵N pattern in marine algae: Tracer potential for cyanobacterial vs. eukaryotic organic nitrogen sources in the ocean. *Geochimica et Cosmochimica Acta*, 103, 104–120.
- McCorkle, D. C., Keigwin, L. D., Corliss, B. H., & Emerson, S. R. (1990). The influence of microhabitats on the carbon isotopic composition of deep-sea benthic foraminifera. *Paleoceanography* 5(2), 161–185.
- M bius, J., Gaye, B., Lahajnar, N., Bahlmann, E., & Emeis, K.-C. (2011). Influence of diagenesis on sedimentary δ¹⁵N in the Arabian Sea over the last 130 kyr. *Marine Geology*, 284, 127–138. <https://doi.org/10.1016/j.margeo.2011.03.013>
- Monnin, E., Steig, E. J., Siegenthaler, U., Kawamura, K., Schwander, J., Stauffer, B., et al. (2004). Evidence for substantial accumulation rate variability in Antarctica during the Holocene, through synchronization of CO₂ in the Taylor Dome, Dome C and DML ice cores. *Earth and Planetary Science Letters*, 224, 45–54.
- Mook, W. G., Bommerson, J. C., & Staverman, W. H. (1974). Carbon isotope fractionation between dissolved bicarbonate and gaseous carbon dioxide. *Earth and Planetary Science Letters*, 22, 169–176.
- Moore, C. M., Mills, M. M., Arrigo, K. R., Berman-Frank, I., Bopp, L., Boyd, P. W., et al. (2013). Processes and patterns of oceanic nutrient limitation. *Nature Geoscience*, 6, 701–710.

- Nozaki, Y., & Yamamoto, Y. (2001). Radium 228 based nitrate fluxes in the eastern Indian Ocean and the South China Sea and silica-induced "alkalinity pump" hypothesis. *Global Biogeochemical Cycles*, *15*, 555–567.
- Olsen, A., Lange, N., Key, R. M., Tanhua, T., Bittig, H. C., Kozyr, A., et al. (2020). An updated version of the global interior ocean biogeochemical data product, GLODAPv2.2020. *Earth System Science Data*, *12*, 3653–3678. <https://doi.org/10.5194/essd-12-3653-2020>
- Olsen, A., & Ninnemann, U. (2010). Large $\delta^{13}\text{C}$ gradients in the preindustrial north Atlantic revealed. *Science*, *330*(6004), 658–659.
- Paytan, A. (2009). Ocean paleoproductivity. In Gornitz, V. (Ed.) *Encyclopedia of paleoclimatology and ancient environments*. *Encyclopedia of Earth Sciences Series*. Springer.
- Paytan, A., & McLaughlin, K. (2011). Tracing the sources and biogeochemical cycling of phosphorus in aquatic systems using isotopes of oxygen in phosphate. In: In M. Baskaran (Ed.), *Handbook of environmental isotope geochemistry* (Vol. 1, p. 419–436). Springer. https://doi.org/10.1007/978-3-642-10637-8_21
- Peters, B. D., Lam, P. J., & Casciotti, K. L. (2018). Nitrogen and oxygen isotope measurements of nitrate along the US GEOTRACES Eastern Pacific Zonal Transect (GP16) yield insights into nitrate supply, remineralization, and water mass transport. *Marine Chemistry*, *201*, 137–150. <https://doi.org/10.1016/j.marchem.2017.09.009>
- Pichevin, L. E., Ganeshram, R. S., & Dumont, M. (2020). Deglacial Si remobilization from the deep-ocean reveals biogeochemical and physical controls on glacial atmospheric CO_2 levels. *Earth and Planetary Science Letters*, *543*, 116332. <https://doi.org/10.1016/j.epsl.2020.116332>
- Pichevin, L. E., Reynolds, B. C., Ganeshram, R. S., Cacho, I., Pena, L., Keefe, K., & Ellam, R. M. (2009). Enhanced carbon pump inferred from relaxation of nutrient limitation in the glacial ocean. *Nature*, *459*, 1114–1117. <https://doi.org/10.1038/nature08101>
- Quay, P., & Wu, J. (2015). Impact of end-member mixing on depth distributions of $\delta^{13}\text{C}$, cadmium and nutrients in the N. Atlantic Ocean. *Deep Sea Research Part II*, *116*, 107–116.
- Rafter, P. A., Bagnell, A., Marconi, D., & DeVries, T. (2019). Global trends in marine nitrate N isotopes from observations and a neural network-based climatology. *Biogeosciences*, *16*, 2617–2633. <https://doi.org/10.5194/bg-16-2617-2019>
- Rafter, P. A., & Charles, C. D. (2012). Pleistocene equatorial Pacific dynamics inferred from the zonal asymmetry in sedimentary nitrogen isotopes. *Paleoceanography*, *27*. <https://doi.org/10.1029/2012pa002367>
- Rafter, P. A., DiFiore, P. J., & Sigman, D. M. (2013). Coupled nitrate nitrogen and oxygen isotopes and organic matter remineralization in the Southern and Pacific Oceans. *Journal of Geophysical Research: Oceans*, *118*, 1–14. <https://doi.org/10.1002/jgrc.20316>
- Rafter, P. A., Sigman, D. M., Charles, C. D., Kaiser, J., & Haug, G. H. (2012). Subsurface tropical Pacific nitrogen isotopic composition of nitrate: Biogeochemical signals and their transport. *Global Biogeochemical Cycles*, *26*, GB1003. <https://doi.org/10.1029/2010GB003979>
- Ren, H., Sigman, D. M., Martínez-García, A., Anderson, R. F., Chen, M.-T., Ravelo, A. C., et al. (2017). Impact of glacial/interglacial sea level change on the ocean nitrogen cycle. *Proceedings of the National Academy of Sciences of the United States of America*, *114*(33), E6759–E6766. <https://doi.org/10.1073/pnas.1701315114>
- Ren, H., Sigman, D. M., Meckler, A. N., Plessen, B., Robinson, R. S., Rosenthal, Y., & Haug, G. H. (2009). Foraminiferal isotope evidence of reduced nitrogen fixation in the ice age Atlantic Ocean. *Science*, *323*, 244–248. <https://doi.org/10.1126/science.1165787>
- Ren, H., Sigman, D. M., Thunell, R. C., & Prokopenko, M. G. (2012). Nitrogen isotopic composition of planktonic foraminifera from the modern ocean and recent sediments. *Limnology & Oceanography*, *57*(4), 1011–1024. <https://doi.org/10.4319/lo.2012.57.4.1011>
- Ren, H., Studer, A. S., Serno, S., Sigman, D. M., Winckler, G., Anderson, R. F., et al. (2015). Glacial-to-interglacial changes in nitrate supply and consumption in the subarctic North Pacific from microfossil-bound N isotopes at two trophic levels. *Paleoceanography*, *30*, 1217–1232. <https://doi.org/10.1002/2014PA002765>
- Richaud, M., Loubere, P., Pichat, S., & Francois, R. (2007). Changes in opal flux and the rain ratio during the last 50,000 years in the equatorial Pacific. *Deep Sea Research Part II*, *54*, 762–771.
- Robinson, R. S., Brzezinski, M. A., Beucher, C. P., Horn, M. G., & Bedsole, P. (2014). The changing roles of iron and vertical mixing in regulating nitrogen and silicon cycling in the Southern Ocean over the last glacial cycle. *Paleoceanography*, *29*, 1179–1195. <https://doi.org/10.1002/2014PA002686>
- Robinson, R. S., Kienast, M., Albuquerque, A. L., Altabet, M., Contreras, S., Holz, R. D., et al. (2012). A review of nitrogen isotopic alteration in marine sediments. *Paleoceanography*, *27*. <https://doi.org/10.1029/2012pa002321>
- Robinson, R. S., Martinez, P., Pena, L. D., & Cacho, I. (2009). Nitrogen isotopic evidence for deglacial changes in nutrient supply in the eastern equatorial Pacific. *Paleoceanography*, *24*(4). <https://doi.org/10.1029/2008pa001702>
- Robinson, R. S., Moore, T. C., Erhardt, A. M., & Scher, H. D. (2015). Evidence for changes in subsurface circulation in the late Eocene equatorial Pacific from radiolarian-bound nitrogen isotope values. *Paleoceanography*, *30*, 912–922. <https://doi.org/10.1002/2015PA002777>
- Robinson, R. S., Sigman, D. M., DiFiore, P. J., Rohde, M. M., Mashiotta, T. A., & Lea, D. A. (2005). Diatom-bound $^{15}\text{N}/^{14}\text{N}$: New support for enhanced nutrient consumption in the ice age subantarctic. *Paleoceanography*, *20*. <https://doi.org/10.1029/2004PA001114>
- Rousseau, J., Ellwood, M. J., Bostock, H., & Neil, H. (2016). Estimates of late Quaternary mode and intermediate water silicic acid concentration in the Pacific Southern Ocean. *Earth and Planetary Science Letters*, *439*, 101–108.
- Rubino, M., Etheridge, D. M., Trudinger, C. M., Allison, C. E., Battle, M. O., Langenfelds, R. L., et al. (2013). A revised 1000 year atmospheric $\delta^{13}\text{C}\text{-CO}_2$ record from Law Dome and South Pole, Antarctica. *Journal of Geophysical Research: Atmospheres*, *118*, 8482–8499. <https://doi.org/10.1002/jgrd.50668>
- Sackett, W. M., Eckelmann, W. R., Bender, M. L., & Bé, A. W. (1965). Temperature dependence of carbon isotope composition in marine plankton and sediments. *Science*, *148*(3667), 235–237.
- Schlitzer, R., Anderson, R. F., Masferrer Dodas, E., Lohan, M., Geibert, W., Tagliabue, A., et al. (2018). The GEOTRACES intermediate data product 2017. *Chemical Geology*, *493*, 210–223.
- Schmittner, A., Gruber, N., Mix, A. C., Key, R. M., Tagliabue, A., & Westberry, T. K. (2013). Biology and air-sea gas exchange controls on the distribution of carbon isotope ratios ($\delta^{13}\text{C}$) in the ocean. *Biogeosciences*, *10*, 5793–5816.
- Schmittner, A., & Lund, D. C. (2015). Early deglacial Atlantic overturning decline and its role in atmospheric CO_2 rise inferred from carbon isotopes ($\delta^{13}\text{C}$). *Climate of the Past*, *11*, 135–152. <https://doi.org/10.5194/cp-11-135-2015>
- Schmittner, A., & Somes, C. J. (2016). Complementary constraints from carbon (^{13}C) and nitrogen (^{15}N) isotopes on the glacial ocean's soft-tissue biological pump. *Paleoceanography*, *31*, 669–693. <https://doi.org/10.1002/2015PA002905>
- Schubert, C. J., & Calvert, S. E. (2001). Nitrogen and carbon isotopic composition of marine and terrestrial organic matter in Arctic Ocean sediments: Implications for nutrient utilization and organic matter composition. *Deep Sea Research Part I*, *48*, 789–810.
- Shackleton, N. J., Hall, M. A., Line, J., & Crag, S. (1983). Carbon isotope data in core V19-30 confirm reduced carbon dioxide concentration in the ice age atmosphere. *Nature*, *306*, 319–322.
- Shemesh, A., Mortlock, R. A., Smith, R. J., & Froelich, P. N. (1988). Determination of Ge/Si in marine siliceous microfossils: Separation, cleaning and dissolution of diatoms and radiolaria. *Marine Chemistry*, *25*, 305–323.

- Sigman, D. M., Altabet, M. A., Francois, R., McCorkle, D. C., & Gaillard, J.-F. (1999). The isotopic composition of diatom-bound nitrogen in Southern Ocean sediments. *Paleoceanography*, *14*(2), 118–134.
- Sigman, D. M., Altabet, M. A., McCorkle, D. C., Francois, R., & Fischer, G. (2000). The $\delta^{15}\text{N}$ of nitrate in the Southern Ocean: Nitrogen cycling and circulation in the ocean interior. *Journal of Geophysical Research: Oceans*, *105*(C8), 19599–19614.
- Sigman, D. M., & Boyle, E. A. (2000). Glacial/interglacial variations in atmospheric carbon dioxide. *Nature*, *407*(6806), 859–869.
- Sigman, D. M., DiFiore, P. J., Hain, M. P., Deutsch, C., & Karl, D. M. (2009). Sinking organic matter spreads the nitrogen isotope signal of pelagic denitrification in the North Pacific. *Geophysical Research Letters*, *36*, L08605. <https://doi.org/10.1029/2008GL035784>
- Sigman, D. M., & Fripiat, F. (2019). Nitrogen isotopes in the ocean. In J. K. Cochran, J. H. Bokuniewicz, & L. P. Yager (Eds.), *Encyclopedia of ocean sciences* (3rd ed., pp. 263–278). Elsevier.
- Sigman, D. M., Fripiat, F., Studer, A. S., Kemeny, P. C., Martínez-García, A., Hain, M. P., et al. (2021). The Southern Ocean during the ice ages: A review of the Antarctic surface isolation hypothesis, with comparison to the North Pacific. *Quaternary Science Reviews*, *254*. <https://doi.org/10.1016/j.quascirev.2020.106732>
- Sigman, D. M., & Hain, M. P. (2012). The biological productivity of the ocean: Section 1, *Nature Education Knowledge*, *3*(10), 21.
- Sigman, D. M., Hain, M. P., & Haug, G. H. (2010). The polar ocean and glacial cycles in atmospheric CO_2 concentration. *Nature*, *466*, 47–55. <https://doi.org/10.1038/nature09149>
- Smart, S. M., Fawcett, S. E., Ren, H., Schiebel, R., Tompkins, E. M., Martínez-García, A., et al. (2020). The nitrogen isotopic composition of tissue and shell-bound organic matter of planktic foraminifera in Southern Ocean surface waters. *Geochemistry, Geophysics, Geosystems*, *21*, e2019GC008440.
- Smart, S. M., Ren, H., Fawcett, S. E., Schiebel, R., Conte, M., Rafer, P. A., et al. (2018). Ground-truthing the planktic foraminifer-bound nitrogen isotope paleo-proxy in the Sargasso Sea. *Geochimica et Cosmochimica Acta*, *235*, 463–482. <https://doi.org/10.1016/j.gca.2018.05.023>
- Somes, C. J., Oschlies, A., & Schmittner, A. (2013). Isotopic constraints on the pre-industrial oceanic nitrogen budget. *Biogeosciences*, *10*, 5889–5910. <https://doi.org/10.5194/bg-10-5889-2013>
- Somes, C. J., Schmittner, A., Galbraith, E. D., Lehmann, M. F., Altabet, M. A., Montoya, J. P., et al. (2010). Simulating the global distribution of nitrogen isotopes in the ocean. *Global Biogeochemical Cycles*, *24*, GB4019. <https://doi.org/10.1029/2009GB003767>
- Somes, C. J., Schmittner, A., Muglia, J., & Oschlies, A. (2017). A three-dimensional model of the marine nitrogen cycle during the Last Glacial Maximum constrained by sedimentary isotopes. *Frontiers in Marine Science*, *4*. <https://doi.org/10.3389/fmars.2017.00108>
- Spero, H. J. (1998). Life history and stable isotope geochemistry of planktonic foraminifera. In *Isotope paleobiology and paleoecology* (pp. 7–36). Paleontological Society.
- Spero, H. J., Bijma, J., Lea, D., & Bemis, B. (1997). Effect of seawater carbonate concentration on foraminiferal carbon and oxygen isotopes. *Nature*, *390*, 497–500.
- Spero, H. J., Mielke, K. M., Kalve, E. M., Lea, D. W., & Pak, D. K. (2003). Multispecies approach to reconstructing eastern equatorial Pacific thermocline hydrography during the past 360 kyr. *Paleoceanography* *18*(1), 1022. <https://doi.org/10.1029/2002PA00814>
- Straub, M., Sigman, D. M., Ren, H., Martínez-García, A., Nele Meckler, A., Hain, M. P., & Haug, G. H. (2013). Changes in North Atlantic nitrogen fixation controlled by ocean circulation. *Nature*, *501*, 200–203. <https://doi.org/10.1038/nature12397>
- Studer, A. J., Sigman, D. M., Martínez-García, A., Benz, V., Winckler, G., Kuhn, G., et al. (2015). Antarctic Zone nutrient conditions during the last two glacial cycles. *Paleoceanography*, *30*, 845–862. <https://doi.org/10.1002/2014PA002745>
- Studer, A. J., Sigman, D. M., Martínez-García, A., Thöle, L. M., Michel, E., Jaccard, S. L., et al. (2018). Increased nutrient supply to the Southern Ocean during the Holocene and its implications for the pre-industrial atmospheric CO_2 rise. *Nature Geoscience*, *11*, 756–760. <https://doi.org/10.1038/s41561-018-0191-8>
- Sutton, J. N., André, L., Cardinal, D., Conley, D. J., de Souza, G. F., Dean, J., et al. (2018). A review of the stable isotope bio-geochemistry of the global silicon cycle and its associated trace elements. *Frontiers of Earth Science*, *5*. <https://doi.org/10.3389/feart.2017.00112>
- Sutton, J. N., Varela, D. E., Brzezinski, M. A., & Beucher, C. P. (2013). Species-dependent silicon isotope fractionation by marine diatoms. *Geochimica et Cosmochimica Acta*, *104*, 300–309. <https://doi.org/10.1016/j.gca.2012.10.057>
- Tappan, H. (1968). Primary production, isotopes, extinctions and the atmosphere. *Palaeogeography, Palaeoclimatology, Palaeoecology*, *4*, 187–210.
- Tesdal, J.-E., Galbraith, E. D., & Kienast, M. (2013). Nitrogen isotopes in bulk marine sediment: Linking seafloor observations with subsurface records. *Biogeosciences*, *10*, 101–118. <https://doi.org/10.5194/bg-10-101-2013>
- Thöle, L. M., Amsler, H. E., Moretti, S., Auderset, A., Gilgannon, J., Lippold, J., et al. (2019). Glacial-interglacial dust and export production records from the Southern Indian Ocean. *Earth and Planetary Science Letters*, *525*. <https://doi.org/10.1016/j.epsl.2019.115716>
- Tréguer, P. J., Sutton, J. N., Brzezinski, M., Charette, M. A., Devries, T., Dutkiewicz, S., et al. (2021). Reviews and syntheses: The biogeochemical cycle of silicon in the modern ocean. *Biogeosciences*, *18*, 1269–1289. <https://doi.org/10.5194/bg-18-1269-2021>
- Tribovillard, N., Algeo, T. J., Lyons, T., & Riboulleau, A. (2006). Trace metals as paleoredox and paleoproductivity proxies: An update. *Chemical Geology*, *232*, 12–32. <https://doi.org/10.1016/j.chemgeo.2006.02.012>
- Tuerena, R. E., Ganeshram, R. S., Geibert, W., Fallick, A. E., Dougans, J., Tait, A., et al. (2015). Nutrient cycling in the Atlantic basin: The evolution of nitrate isotope signatures in water masses. *Global Biogeochemical Cycles*, *29*, 1830–1844. <https://doi.org/10.1002/2015GB005164>
- Turner, S. K. (2014). Pliocene switch in orbital-scale carbon cycle/climate dynamics. *Paleoceanography*, *29*, 1256–1266. <https://doi.org/10.1002/2014PA002651>
- Umling, N. E., & Thunell, R. C. (2018). Mid-depth respired carbon storage and oxygenation of the eastern equatorial Pacific over the last 25,000 years. *Quaternary Science Reviews*, *189*, 43–56.
- Varela, D. E., Pride, C. J., & Brzezinski, M. A. (2004). Biological fractionation of silicon isotopes in Southern Ocean surface waters. *Global Biogeochemical Cycles*, *18*, GB1047. <https://doi.org/10.1029/2003GB002140>
- Volk, T., & Hoffert, M. I. (1985). Ocean carbon pumps: Analysis of relative strengths and efficiencies in ocean-driven atmospheric CO_2 changes. In E. T. Sundquist, W. S. Broecker (Eds.), *The carbon cycle and atmospheric CO_2 : Natural variations Archaean to present. Geophysical Monographic Series* (Vol. 32, 99–110). American Geophysical Union.
- Wada, E. (1980). Nitrogen isotope fractionation and its significance in biogeochemical processes occurring in marine environments. In E. D. Goldberg, Y. Horibe, K. Saruhashi (Eds.), *Isotope marine chemistry* (pp. 375–398). Geochemistry Research Association.
- Walker, J. D., Geissman, J. W., Bowring, S. A., & Babcock, L. E. (2018). *Geologic time scale v. 5.0*. Geological Society of America.
- Wang, X. T., Prokopenko, M. G., Sigman, D. M., Adkins, J. F., Robinson, L. F., Ren, H., et al. (2014). Isotopic composition of carbonate-bound organic nitrogen in deep-sea scleractinian corals: A new window into past biogeochemical change. *Earth and Planetary Science Letters*, *400*, 243–250. <https://doi.org/10.1016/j.epsl.2014.05.048>

- Wang, X. T., Sigman, D. M., Prokopenko, M. G., Adkins, J. F., Robinson, L. F., Hines, S. K., et al. (2017). Deep-sea coral evidence for lower Southern Ocean surface nitrate concentrations during the last ice age. *Proceedings of the National Academy of Sciences of the United States of America*, 114(13), 3352–3357. <https://doi.org/10.1073/pnas.1615718114>
- Waser, N. A. D., Harrison, P. J., Nielsen, B., Calvert, S. E., & Turpin, D. H. (1998). Nitrogen isotope fractionation during the uptake and assimilation of nitrate, nitrite, ammonium, and urea by a marine diatom. *Limnology & Oceanography*, 43, 215–224.
- Wetzel, F., de Souza, G. F., & Reynolds, B. C. (2014). What controls silicon isotope fractionation during dissolution of diatom opal? *Geochimica et Cosmochimica Acta*, 131, 128–137. <https://doi.org/10.1016/j.gca.2014.01.028>
- Wille, M., Sutton, J., Ellwood, M. J., Sambridge, M., Maher, W., Eggins, S., & Kelly, M. (2010). Silicon isotopic fractionation in marine sponges: A new model for understanding silicon isotopic variations in sponges. *Earth and Planetary Science Letters*, 292(3–4), 281–289. <https://doi.org/10.1016/j.epsl.2010.01.036>
- Woodruff, F., Savin, S., & Douglas, R. G. (1980). Biological fractionation of oxygen and carbon isotopes by recent benthic foraminifera. *Marine Micropaleontology*, 5, 3–11.
- Xiong, Z., Li, T., Algeo, T., Doering, K., Frank, M., Brzezinski, M. A., et al. (2015). The silicon isotope composition of *Ethmodicus rex* laminated diatom mats from the tropical west Pacific: Implications for silicate cycling during the Last Glacial Maximum. *Paleoceanography*, 30, 803–823. <https://doi.org/10.1002/2015PA002793>
- Zachos, J. C., Dickens, G. R., & Zeebe, R. E. (2008). An early Cenozoic perspective on greenhouse warming and carbon-cycle dynamics. *Nature*, 451, 279–283.
- Zachos, J. C., Flower, B. P., & Paul, H. (1997). Orbitally paced climate oscillations across the Oligocene/Miocene boundary. *Nature*, 388, 567–570.
- Zachos, J. C., Pagani, M., Sloan, L., Thomas, E., & Billups, K. (2001). Trends, rhythms, and aberrations in global climate 65 Ma to present. *Science*, 292, 686–693. <https://doi.org/10.1126/science.1059412>
- Zhang, J., Quay, P. D., & Wilbut, D. O. (1995). Carbon isotope fractionation during gas-water exchange and dissolution of CO₂. *Geochimica et Cosmochimica Acta*, 59, 107–114.
- Ziegler, M., Diz, P., Hall, I. R., & Zahn, R. (2013). Millennial-scale changes in atmospheric CO₂ levels linked to the Southern Ocean carbon isotope gradient and dust flux. *Nature Geoscience*, 6, 457–461. <https://doi.org/10.1038/ngeo1782>